Physics – Uspekhi **66** (11) 1071 – 1094 (2023)

REVIEWS OF TOPICAL PROBLEMS PACS numbers: **26.30. – k**, 95.30.Lz, **98.38. – j**, **98.58. – w**, 98.62.Ra

Initial episodes of the chemical evolution of the intergalactic medium

Yu A Shchekinov, E O Vasiliev, B M Shustov

DOI: https://doi.org/10.3367/UFNe.2022.12.039295

Contents

Abstract. The current state of the problem of the origin and transport of 'heavy' ($A > 4$) chemical elements in the Universe is discussed. The beginning of stellar nucleosynthesis (SNS) dates apparently to $z \gtrsim 20$ redshift epochs (age of the Universe $t_U \lesssim 180$ Myr). Presently, SNS traces are observed in some cases in galaxies at redshift $z \sim 10-15$ ($t_U \sim 500-270$ Myr). A massive redistribution of chemical elements from galaxies over the entire Universe became possible, primarily under the action of powerful explosions, in the reionization period at $z \lesssim 6$ ($t_U \gtrsim 940$ Myr). A correct interpretation of observational data requires an in-depth understanding of the transport and mixing dynamics of chemical elements in the Universe. Theoretical models predict their extremely nonuniform distribution in a range from the interstellar medium on spatial scales of a few hundred light years to the intergalactic medium spanning tens of millions of light years. This is observed in absorption spectra of quasars up to redshift $z \sim 6$ and results in observational selection. The review focuses on the early stages of the history of the Universe's chemical enrichment as it is currently understood given the observational selection effects. Observational data and theoretical ideas underlying the modern understanding of the complex process of the Universe's chemical evolution are outlined.

Keywords: Universe, intergalactic medium, galaxies, interstellar medium, chemical elements, transport

1. Introduction

The origin of chemical elements in the Universe is one of the basic riddles. The history of the issue goes back to the classic work of G A Gamow, C F von Weizsäcker, H Bethe, and S Chandrasekhar that appeared 80 years ago [1–4]. It is now well known that the primordial baryonic matter in the Universe contained only the lightest chemical elements, no heavier than lithium (see a review of the current state in [5]). The emergence of heavier elements[1] is a result of nucleosynthesis in the interiors of stars [6–10].

It is now established that the interior of stars is the birthplace of at least 90 chemical elements known to us; the rest of the elements are artificial.[2] During their evolution, stars eject heavy elements into the interstellar medium (ISM). During the active 'bursts' of star formation, some metals are ejected from galaxies into intergalactic space (the Intergalactic Medium, IGM). This is, in general terms, the scenario for the redistribution of metals throughout the Universe.

Yu A Shchekinov [1,2,a], **E O Vasiliev** [1,3,b], **B M Shustov** [3,c]
[1] Lebedev Physical Institute, Russian Academy of Sciences, Leninskii prosp. 53, 119991 Moscow, Russian Federation
[2] Raman Research Institute, C. V. Raman Avenue, Sadashiva Nagar, Bangalore, 560080, India
[3] Institute of Astronomy, Russian Academy of Sciences, ul. Pyatnitskaya 48, 119017 Moscow, Russian Federation
E-mail: [a] yus@asc.rssi.ru, [b] eugstar@mail.ru, [c] bshustov@inasan.ru

Received 26 September 2022, revised 6 December 2022
Uspekhi Fizicheskikh Nauk **193** (11) 1137 – 1161 (2023)
Translated by M Zh Shmatikov

[1] Below, along with the term 'heavy elements,' the name 'metals' accepted in astrophysics is also used.
[2] https://en.wikipedia.org/wiki/Chemical_element.

Based on intuitive ideas, we hypothesize a simple correspondence between the age of a star and the number of heavy elements it contains: the fewer heavy elements observed in a star, the earlier in the Universe it was formed. However, such a straightforward understanding is not indisputable. If an individual star is considered, its chemical composition only reflects the conditions in the cloud of gas from which the star arose. In a galaxy, the number and composition of heavy elements in individual ISM regions may be a result of a superposition of 'imprints' of several enrichment episodes that occurred in the galaxy throughout its evolution. The understanding of this complex picture is often obscured by observational selection effects. Even if we are considering the values averaged over a fairly large ensemble of galaxies, the amount of metal in stellar systems can be used as an indicator of their age, with strong reservations, since root-mean-square deviations are always very large (a good analysis of the observational aspects of determining the relationship between metallicity and age is presented in study [11] and in review [12]). A recent examination of this relationship in our Galaxy's disk [13] based on a sample of 189 binary stars of presumably the same age (with a white dwarf as one of the companions), using the Gaia project's second data release (DR2), yielded a dispersion of metallicity of more than half an order of magnitude with a relative measurement error $\Delta Z/Z \lesssim 0.7$ (Z is the relative mass content of metals). Moreover, the authors of [13] emphasize that no evolutionary trend is observed in a span of over 9 Gyr (see the upper-right panel in Fig. 4 in [13]).

Quite recently, a comprehensive analysis of a large sample (more than 36,000) of low-metallicity stars in our Galaxy [14] has made it possible to identify a group of approximately 7,000 stars with metallicity[3] varying in a wide range of $3 \times 10^{-4} < \zeta < 0.15$, the phase space of which does not overlap with that of the entire sample (see Fig. 5 in [14]). Apparently, this group is a kinematically isolated stellar disk of the same age — the authors of [14] call it the Atari disk. This observation makes the question of the early chemical evolution of our Galaxy even more challenging.

On the other hand, observations of early galaxies (i.e., galaxies at the stage of emergence or early evolution) in the redshift range $z \sim 5-7$ exhibit metal contents $Z \sim 0.2-0.5Z_\odot$ [15–19], comparable to that in *galaxies that evolved* more than a billion years later to $z \sim 1-2$ [19, 20]. This dispersion implies that the mixing of matter in the Galaxy (the same refers to other galaxies) does not provide a uniform chemical composition that would correspond to the expected increase in metallicity with age. Therefore, studying the mixing of metals during the galactic evolutionary process is of fundamental importance.

Heavy elements are distributed throughout all baryonic structural components of the Universe. About 10% of the mass of heavy elements at $z \sim 4-6$ is apparently contained neither in stars nor in the ISM, but in the IGM, in the Circumgalactic Medium (CGM), and in the gas of galaxy clusters (Intracluster Medium, ICM). Assuming that half of the stars in galaxies feature solar metallicity and taking into account that the density parameter of *stellar* matter in the Universe[4] is $\Omega_* \approx 0.004$ [21], we can obtain an estimate for the density parameter of metals in stars: $\Omega_{Z_*} \sim 4 \times 10^{-5}$. The total density parameter of metals outside galaxies is of the order of $\Omega_{Z,\mathrm{ex}} \sim 6 \times 10^{-5}$. Here, for intergalactic and circumgalactic gas and gas in clusters, the values $\Omega_{\mathrm{IGM}} \approx 0.016$, $\Omega_{\mathrm{CGM}} \approx 0.024$, and $\Omega_{\mathrm{ICM}} \approx 0.0018$ [21] are accepted, and their metallicities are taken to be $\zeta_{\mathrm{IGM}} \approx 0.001$, $\zeta_{\mathrm{CGM}} \approx 0.1$, and $\zeta_{\mathrm{ICM}} \approx 0.3$ [22–25], respectively.

In this review, we discuss the possible mechanisms that lead to such striking disagreement between the observed relationships between the age of stellar systems and their metallicity and intuitive expectations. One of them is associated with the mechanisms of transfer of metals from their sources, stars, to the scale of galaxies and intergalactic space. Therefore, we mostly focus on the enrichment of metals in that part of the Universe that is located outside the galaxies, where the problem of transfer manifests itself most clearly.

2. Galaxy and local Universe

2.1 Stellar populations of the Galaxy

The very first concepts of the Universe's chemistry were based on studies of the immediate vicinity of the Sun. Stellar populations of the Galaxy are conventionally separated into three types of different ages[5]: (1) population I — the modern population of the stellar disk with a metallicity of the order of solar one ($\zeta \approx 0.25-1$) and age $t_{\mathrm{I}} \leqslant 10$ Gyr (corresponding to $z \leqslant 1.8$); (2) population II — an older population, which includes a thick disk ($\zeta \approx 0.2-0.6$ and $t_{\mathrm{II,d}} > 10$ Gyr, $z > 1.8$) and stars of the spherical subsystem ($\zeta \approx 0.02$ and $t_{\mathrm{II,h}} > 12$ Gyr, $z \approx 3.6$) [27–30]; and (3) also, apparently, stars of population II.5 preceding them with metallicity $Z/Z_\odot < 0.01$ [31, 32], enriched in metals produced by the very first stars in the Universe — population III stars formed from the primordial matter. The oldest stellar populations are represented exclusively by low-mass stars, $M \leqslant 0.8M_\odot$, since the lifetime of more massive stars is shorter than the age of the Universe.

Figure 1 illustrates the relationship between the metallicities of stellar populations of various ages. As noted above, the age–metallicity relationship is virtually nonexistent for stars younger than $t_* \leqslant 9$ Gyr. However, the oldest stars, $9 < t_* < 13.7$ Gyr, exhibit a sharp decrease in metallicity, although with a large (by two orders of magnitude) dispersion for the same age. The light-green band in Fig. 1 displays the region of metallicities measured in early galaxies and the intergalactic medium[6] in the redshift range from $z \approx 0.15$ to $z \approx 6$. It is easy to see a noticeable 'lag' in the apparent chemical evolution of young galaxies in the distant ($z > 0.1$) Universe behind our Galaxy at the same epochs of the Universe.

[3] In astrophysics, the term 'metallicity' of astronomical objects is understood as the relative density of heavy elements in these objects $\zeta = Z/Z_\odot$, where Z is the mass fraction of heavy elements. For the Sun, $Z_\odot = 0.018$. Observers often call 'metallicity' the logarithm of the ratio $[X/\mathrm{H}] = \lg(X/\mathrm{H}) - \lg(X/\mathrm{H})_\odot$, where X denotes a chemical element: Fe (most often) or O, Ca, and C.

[4] $\Omega_* = \rho_*/\rho_{\mathrm{c}}$, where ρ_* is the density of matter contained in stars, $\rho_{\mathrm{c}} = 3H^2/8\pi G$ is the critical density, H is the Hubble constant, and G is the gravitational constant.

[5] It should be taken into consideration that determining the ages of stars per se is an extremely complex problem, and the uncertainty in ages obtained by different methods can be as large as 50% or even more (see detailed review [26]).

[6] Saturated Lyα lines of atomic hydrogen with a column density $N(\mathrm{HI}) \geqslant 2 \times 10^{20}$ cm^{-2}, DLA systems, are associated with young galaxies, while optically thin Lyα lines, the Lyα forest, correspond to absorption in the intergalactic medium.

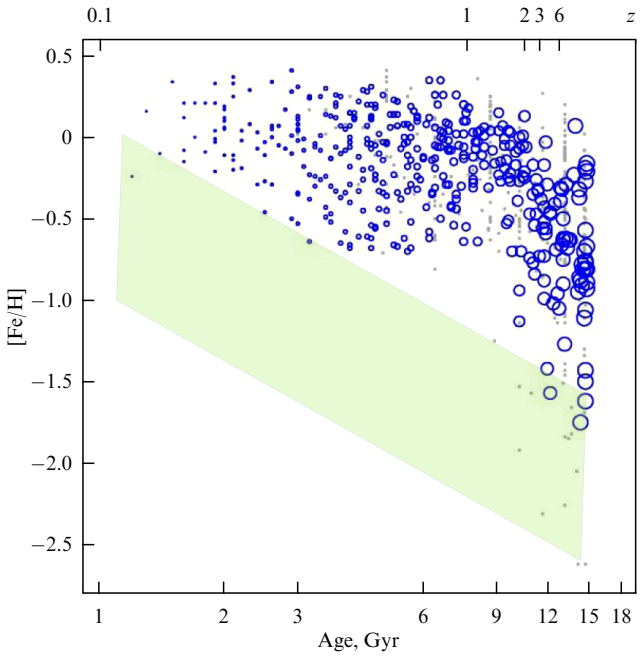

Figure 1. Abundance of chemical elements in the stellar populations of our Galaxy (Milky Way); x-axis indicates the age of stars. Top axis shows the redshift corresponding to the moment of star formation. Vertical axis indicates the metallicity indicator [Fe/H]. Sizes of the circles correspond to the age of the stars; some stars with a large error in age are shown as small gray dots. For comparison, the region corresponding to observations of metallicity in saturated Lyα systems and in Lyα forest lines is shaded. (Figure adapted from [11].)

Such a difference may be a result of either a single 'burst' of activity in our Galaxy due, as is believed, to its merging with a galaxy of lower mass [11, 33, 34], or a consequence of multiple sporadic surges in the star formation rate when it absorbed dwarf bursts in the epoch $z \sim 1-2$ (see discussion in reviews [12, 35]). It should, however, be taken into account that such an interpretation may be plagued by possible effects of observational selection in determining the chemical composition of early galaxies due to insufficient mixing of chemical inhomogeneities (see discussion in Section 7) and the possibility noted above that, during the evolution of the Galaxy, stars of the same age emerge in various regions of the interstellar medium from matter with different chemical compositions.

The oldest stellar population of the Galaxy is presented in Fig. 1 by stars with extremely low metallicity,[7] $\zeta < 10^{-3}$ (see [36, 37]). The minimum known metallicity among them is $\zeta < 10^{-5.3}$ [38, 39]. Stars with a primordial chemical composition, i.e., $Z = 0$, have not yet been discovered in our Galaxy. This fact was in line with the concept that prevailed until recently, according to which only massive population III stars with $M_{\rm III} \gtrsim 10-130\,M_\odot$ can be formed [40–47]. This conclusion was based on calculations of molecular chemistry and the thermal regime of the primordial gas during the formation of the first galaxies. As a consequence of this conclusion, the mass distribution function of emerging stars[8] is shifted towards massive stars, the so-called top-heavy IMF. According to it, population III stars with $Z = 0$ cannot be present in the Galaxy in their primordial form due to their lifetime being too short: $\tau_*(M) \sim 10^{10}(M/M_\odot)^{-5/2}$ years [48]. The origin of EMP stars remains an enigma. Their existence could be justified by assuming that the addition of a minimum (threshold) amount of heavy elements to the primordial gas is capable of transforming the IMF to a 'normal' form with a lower limit of stellar mass $M_{\rm min} \lesssim 0.8\,M_\odot$ (see discussion in [49–52]). This assumption is consistent with the observation that stars born after (and/or under the influence of) population III stars can feature a wide range of metallicities due to ineffective mixing [53–55].

Moreover, radiation losses due to HD molecules can significantly enhance the cooling of the gas and enable the formation of low-mass stars, $M \lesssim M_\odot$ [56–59]. In addition, the influence of a weak field of ionizing radiation from the very first stars and cosmic rays from the first quasars and/or of cosmological origin significantly changes the thermodynamics of gas with a primordial chemical composition [60–65], which also enables the formation of stars with a smaller mass, $M \sim 0.1-0.01\,M_\odot$, without preliminary enrichment of the medium with heavy elements.

Recent numerical calculations [66] have shown that the mass distribution of stars is highly sensitive to the details of the turbulence spectrum on small scales. Depending on the predominance of rotational or potential perturbations, the masses of emerging stars can vary widely from $10^{-2}\,M_\odot$ to $\sim 10\,M_\odot$. Therefore, it cannot be ruled out that EMP stars belong to population III, i.e., originate from primordial matter, and the insignificant amount of metal observed in them is explained by the accretion of enriched matter onto their surface at subsequent stages [67]. This option is supported by recent calculations of variations in the chemical composition in the surface layers of such stars [68]. Recently, even those scenarios in which EMP stars can be formed in the era of cosmological nucleosynthesis have been discussed [69, 70]. This issue remains debatable.

The paper [71] presents arguments in favor of the hypothesis that examination of the relative abundance of heavy elements in stars with extremely low metallicity $Z < 10^{-3}Z_\odot$ makes it possible to 'decode' the history of the early, starting from $z \gtrsim 10$, enrichment of the Galaxy's matter. However, such a procedure may be plagued by the possible influence of the enrichment of the surface layers of EMP stars with massive stars of evolutionary groups of late epochs $z < 2$, which is noted in [67, 68].

2.2 Metals in dwarf galaxies

Outside the Galaxy, the initial episodes of nucleosynthesis are represented by dwarf galaxies in the local Universe.[9] In low-mass galaxies, fewer periods of star formation are expected, so it is easier to separate stellar populations in them and detect traces of enrichment in the first stars. Among the variety of dwarf galaxies, the most suitable for searching for traces of enrichment are ultra-faint dwarf galaxies (UDGs), in which dark matter is dominant: the mass-to-luminosity ratio[10] is $M/L \sim 140-1700$, their luminosity is low, $L \lesssim 3 \times 10^3\,L_\odot$, and the average metallicity of stars, $\zeta \lesssim 0.01$ [72], is close to that of globular clusters of the Galaxy, one of its oldest populations [73]. In addition to low metallicity, the very existence of UDGs indicates their origin in the early epochs ($z > 6-7$) of the Universe, since, due to the action of photoionization and the evaporation of the gas component

[7] Referred to below as EMP (extremely metal-poor).
[8] Initial Mass Function (IMF).
[9] Local Universe is the nearby region within a radius of $R < 300$ Mpc ($z < 0.1$).
[10] Measured in solar units $M_\odot/L_\odot$.

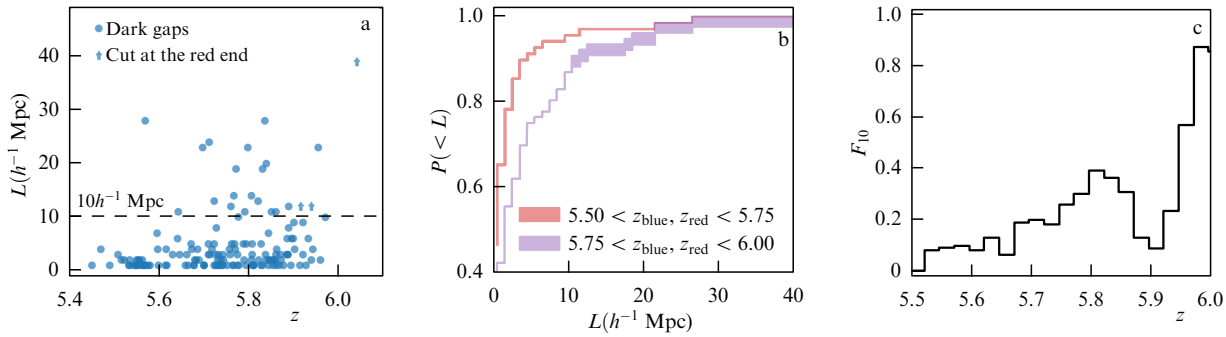

Figure 2. (a) Sizes of the 'depressions,' regions of strong absorption (in the comoving system) in absorption spectra in the Lyβ line in the redshift range $z = 5.4-6.2$; (b) cumulative distribution function of sizes of 'depressions'; (c) fraction of 'depressions' with a size greater than $10h^{-1}$ Mpc, depending on the redshift. (Figures taken from [100].)

associated with it [74, 75], their emergence at later times is hindered. The large spread of metallicity in UDGs ($\sigma_\zeta \sim 1.5-3.0$, see [76]) may be due to the instability of the balance between the outflows of metals from the galaxy and the inflows of matter from the surrounding space, since it depends on only a few events of supernova explosions in one or another direction (see review [77]).

Due to the low mass of gas and, as a consequence, low loss of momentum and energy, even a small number of supernova explosions in ultra-faint dwarf galaxies lead to the ejection of metal-enriched gas into the surrounding IGM (see, for example, [74]). This contributes, on the one hand, to the replenishment of the IGM with metals, and, on the other hand, to the suppression of further star formation (SF) in the host galaxy. The latter circumstance leads to long intervals between successive SF episodes, spanning in some cases to 10 to 12 Gyr [78]. Therefore, ultra-faint dwarf galaxies are the subject of study in 'cosmic archaeology' [79].

The intensity of shock waves in the ISM of ultra-faint dwarf galaxies is weak due to rare episodes of SF, and therefore the mixing of enriched matter in them is ineffective. As a result, the search for chemically peculiar stars in ultra-faint dwarf galaxies is simplified [80]. A nice example is star AS0039 with metallicity $\zeta = 10^{-4.11}$ in the Sculptor galaxy [81], which, unlike the EMP stars in our Galaxy, is not over-enriched in carbon: $N_{\rm C}/N_{\rm Fe} = 10^{-0.75}(N_{\rm C}/N_{\rm Fe})_\odot$, and, moreover, the carbon content turns out to be the lowest among known stars: $N_{\rm C}/N_{\rm H} = 1.5 \times 10^{-5}(N_{\rm C}/N_{\rm H})_\odot$, and it also features a deficiency of α-elements. All these features indicate the formation of this star from matter enriched by a hypernova with zero metallicity — a population III star [80].

Due to their low surface brightness, ultra-faint dwarf galaxies are detectable in emission in only the local Universe [82] and actually turn out to be laboratories for studying the mixing of metal-enriched matter. Taking into account that UDGs are apparently relics of the reionization era, it might be assumed that they can be observed in the absorption spectra of quasars as systems with saturated Lyα lines with $N({\rm HI}) \geqslant 2 \times 10^{20}$ cm^{-2} (damped Lyα, DLA). However, an analysis of the abundances of zinc, sulfur, and oxygen in the dwarf galaxy Sculptor, one of the Galaxy's satellites [83], and in a sample of DLA systems in the redshift range $0.5 \lesssim z \lesssim 3$ [84] showed a significant difference between their SF histories. It should be noted, however, that a comparison of the chemical composition in the ISM of an individual dwarf galaxy and in the peripheral regions of early galaxies, DLA systems, can hardly be a convincing argument. The reason is that the chemical composition of gas at large distances from the centers of galaxies is determined by the activity of large ensembles of supernovae, in contrast to the local enrichment of ISM by individual supernovae in ultra-faint dwarf galaxies [85–87].

3. Metals in the distant Universe

3.1 Reionization and the onset of stellar nucleosynthesis

The first stars and black holes (BHs), which are presumably formed at redshifts $\gtrsim 20$, generate radiation capable of ionizing the Universe. After a long period of 'dark ages,' the hydrogen reionization era begins, which ends in the redshift range $z \sim 5-6$. The first direct observations of quasars in the specified redshift range showed a sharp — approximately by an order of magnitude — decrease proportionally atomic hydrogen at $z \approx 5.5$ [22, 88–93], in line with the expectations of theorists [94–96]. From the onset of reionization at $z \gtrsim 20$ with the appearance of the first stars and black holes and until its completion at $z < 5.5$, when hydrogen becomes almost completely ionized, about 850 Myr elapsed. During this time, the ionization zones around galaxies and black holes expanded and reached intergalactic scales. In the redshift range $5.5 \leqslant z \leqslant 6$, they begin to overlap, and the IGM becomes transparent in the Lyα line of hydrogen [97–99].

A time scan of this period was obtained recently in observations of the 'Lyβ-forest,' which enabled the discovery of gigantic — up to $30h^{-1}$ Mpc — absorption regions ('depressions') in the Lyβ line with an effective optical thickness of $\tau_{\rm GP} \gtrsim 6$ separated by low-absorption 'gaps' [100] (Fig. 2). Figure 2a shows the sizes of the 'depressions'; for some of the depressions at $z \gtrsim 6$, arrows show the sizes of their walls from the 'red' side. Figure 2b presents the cumulative distribution function of depression sizes for two redshift ranges. Figure 2c displays the z-dependence of the fraction of quasars, in the spectra of which 'depressions' with sizes exceeding $10h^{-1}$ Mpc are visible. It can be easily seen that all three indicators show a significant decrease in the size of the 'depressions' at $z \lesssim 5.75$. The reionization dynamics is also clearly visible in the transition to a state of almost complete ionization of hydrogen ($\langle f_{\rm HI}\rangle \tau_{\rm GP} < 5 \times 10^{-5}$) at $z \lesssim 5.5$ and a sharp increase in the effective optical thickness on the Lyα line: $\tau_{\rm GP} \propto (1+z)^{>10.9}$ in the region $z = 5.5-6.3$

(see, for example, [101]). A more detailed review of the reionization history is presented in [102–105].

The onset of reionization and that of stellar nucleosynthesis coincide. This may be evidenced by the hydrogen ionization at redshifts $z \gtrsim 7$ being due predominantly to young 'Lyman break galaxies' (LBGs) [106], the history of which begin at redshifts $z > 10$ [107]. Apparently, the enrichment of the 'entire' IGM with heavy elements, in the sense that the regions of enriched intergalactic gas overlap and form a 'percolating' medium, cannot occur before complete reionization. This is due to the fact that matter is transported by only hydrodynamic flows, which are always slower than the penetration of ionizing radiation into the intergalactic gas. Therefore, the redshifts corresponding to the onset of complete reionization, $z \sim 6$, when regions of gas ionized by individual sources 'percolate,' represent the upper boundary for the onset of the enrichment of *intergalactic space* with metals (see the remark at the conclusion of [108]). In this regard, the detection of singly ionized carbon CII and atomic oxygen OI in the IGM at redshift $z \gtrsim 6$ [109], which may represent isolated regions of ionization from separate sources, seems to be of importance.

The existence of an upper limit on the values of z at which metals enter the IGM, of course, does not exclude the possibility of *local* enrichment of individual regions of gas in the vicinity of galaxies or inside them long before reionization. Recently, observational evidence of *local* enrichment in galaxies at $z \gtrsim 10$ with metallicity $\zeta \sim 0.1$ has appeared [110, 111]. Manifestations of local over-enrichment in the vicinity of quasars are also well known [112–114], including those pertaining to the pre-reionization era ($z > 6.5$, $t_U < 0.8$ Gyr [115, 116]). One of the reasons may be associated with the increased density of matter in the central regions of galaxies and the growth of the minimum mass of IMF stars up to several solar masses [117]. Subsequently, local enrichment can propagate over a larger volume. In this case, it is natural to expect extreme inhomogeneity in the distribution of metals in the IGM, along with the pattern of intermittency of the regions of ionized and atomic gas during the process of reionization (see [118, 119]).

3.2 Galaxies at the dawn of nucleosynthesis

In theoretical scenarios of primordial stellar nucleosynthesis, the latter can begin[11] at $z = 15-20$ (see discussion in [120–123]). The first traces of such *local* enrichment in the epochs long before reionization ($z > 6$) within galaxies and their close circumgalactic neighborhoods were identified in the absorption spectra of optical afterglows of gamma-ray bursts up to $z = 8$ (GRB 090423 [124]). Given that lines of heavy elements are visible in the spectrum of GRB 090423 (for example, the SiIV and FeII lines in GRB 090423), it may be assumed that the *local* enrichment of the Universe with metals apparently began before the GRB 090423 gamma-ray burst.

Recently, the possibility of even earlier episodes of nucleosynthesis has been confirmed by deep surveys conducted in the near-infrared (IR) region of the spectrum and observations made with the JWST (James Webb Space Telescope). Examples include the discovery of the galaxy GN-z11 with (spectroscopic) redshift $z \approx 11$ as part of the CANDELS/GOODS[12] program [110, 111] and two candidate galaxies with (photometric) redshift $z \approx 13$ as part of the HSC SSP Survey[13] [125]. The metallicity of the stellar population and interstellar medium in GN-z11 is estimated to be $\zeta = Z/Z_\odot \sim 0.2$ [110, 111].

The very first results from the JWST pushed the boundaries of the onset of stellar nucleosynthesis even further into the depths of the Universe. Quite recently, the authors of [126] obtained evidence with the JWST of the existence of massive galaxies $M_* \sim 10^9 M_\odot$ at redshift $z \simeq 16-17$ (the Universe's age $t_U \sim 230$ Myr). The result obtained may indicate that during these epochs about half of the baryon mass of galaxies converted into stars in accordance with the model described earlier in [120]. Such a high efficiency of SF could be related to the absence of its suppression by ultraviolet radiation from stars, contrary to general expectations [126]. In cases where the age of stellar populations in such galaxies can be estimated, as, for example, is the case of the Maisie galaxy with redshift $z \simeq 14$ and a stellar age of ~ 150 Myr, described in [127], the moment of its birth can be attributed to redshifts $z > 20$. Quite unexpected was the extremely high metallicity of the matter of galaxies in these epochs, measured to date by indirect methods: in young galaxies at $z \simeq 10-16$, its value estimated by the authors of [128] is $\zeta \sim 0.01-0.1$.

An interesting, albeit indirect, indication of very early episodes of star formation is the discovery of supermassive black holes (SMBHs) with masses comparable to the values in the local Universe $M_{BH} \sim 10^8-10^9 M_\odot$, at redshifts $z \gtrsim 7$, i.e., in the epoch when the Universe's age was less than a billion years [129–131]. Certainly, the formation of such monster SMBHs requires their masses to grow with the Eddington accretion rate, starting at least from redshift $z \gtrsim 30$ [130, 132]. Moreover, their rapid growth should be accompanied by active star formation since, first, only galaxies with a dynamic mass $M_{dyn} \gtrsim 50-500 M_{BH}$ can contain such a massive BH at their center [133] and, second, this rapid growth of such BHs should occur in a fairly massive 'reservoir' of cold molecular gas, the mass of which can reach $M \gtrsim 10^{10} M_\odot$ [134]. These conditions correspond to a high rate of star formation, up to $1000 M_\odot$ yr^{-1}, and a high rate of metal production [135]. The estimated metallicity of the gas in the central regions ($r \sim 1$ kpc) of galaxies containing such BHs is close to or exceeds the solar value.

4. 'Global' enrichment of the Universe

Having begun in the earliest epochs at the end of the 'dark' era, the birth and activity of stars become increasingly intense along with the formation of large-scale structure in the Universe, until reaching the maximum at redshifts $z \sim 2-3$ [136, 137]. By this time, those structural units and topological features appear in the Universe that persist in it to this day. The pattern of chemical evolution of the Universe was apparently modulated by the physical environment associated with the development of structure.

Since nucleosynthesis in these epochs is driven by rapidly evolving massive stars, the early enrichment scenario proceeds in the regime of synchronized large-scale SF bursts with the ejection of heavy elements on a very short time scale $\tau_* \sim 2$ Myr under the assumption of 'top-heavy' IMF with star mass $M_* \sim 30 M_\odot$. Based on this observation, it can be assumed that the era of nucleosynthesis and enrichment of the

[11] It should be emphasized that this refers to the initial episodes of nucleosynthesis, which is essentially *local*.

[12] Cosmic Assembly Near-infrared Deep Extragalactic Legacy Survey/Great Observatories Origin Deep Survey.

[13] Hyper Supreme-Cam Subaru Strategic Program Survey.

galaxies themselves and their close surroundings began simultaneously. As noted above in Section 2.2, the binding energy of low-mass galaxies is low, so just a few supernovae are sufficient to eject a significant part of the gas from the galaxy and stop further star formation [138]. Such a short episode, however, turns out to be sufficient to ensure minimal 'pollution' of the nearest (within 100 kpc) Universe to the level $Z = 10^{-4} Z_{\odot}$ [118, 139–141]. Here, however, it should be kept in mind that such estimates are based on averaging over large (~ 10 Mpc) volumes (see the detailed discussion of these aspects in review [138]) and should only be understood in terms of average values.

The level of 'pollution' with metals $Z \sim 10^{-3}$–$10^{-2}\, Z_{\odot}$ observed in the IGM at redshifts $z \sim 2-5$ may be due to a greater extent to the activity of more massive galaxies in pre-reionization epochs at $z \gtrsim 6$ (see Fig. 14 in [142]).

As noted above, $z \simeq 6$ is the upper limit for the redshifts at which products of stellar nucleosynthesis begin to intensively propagate from the circumgalactic region into the IGM. The surface filling factor of IGM regions occupied by heavy elements increases [152], and some of the enriched regions contribute to absorption. As follows from observations on the CIV and SilV ion lines [22, 151, 153], the z-dependence of the averaged metallicity of intergalactic gas in the region $z \sim 2-5$ turns out to be fairly flat (Figs 3 and 4), which can be associated with the lack of effective mixing by gas-dynamic flows. In the region of redshifts $z < 2.5$, the number of CIV and SilV ions increases sharply, by almost an order of magnitude [151, 154]. The reason may be either an absolute increase in the mass of heavy elements in the Universe and in the IGM during the peak of star formation at $z = 2-4$ [137], or a change in the ionization state of carbon in particular, i.e., a shift in the ionization equilibrium towards CIV ions.

4.1 Universe in absorption lines

The main observational information about the chemical composition of objects in the Universe is provided by observations of absorption spectra. Today's progress in understanding the chemical evolution of the Universe is largely due to the progress in ultraviolet (UV) astronomy. This is explained by the fact that the main absorption lines of heavy-element ions, which are used as indicators of chemical composition, are located in the UV region.

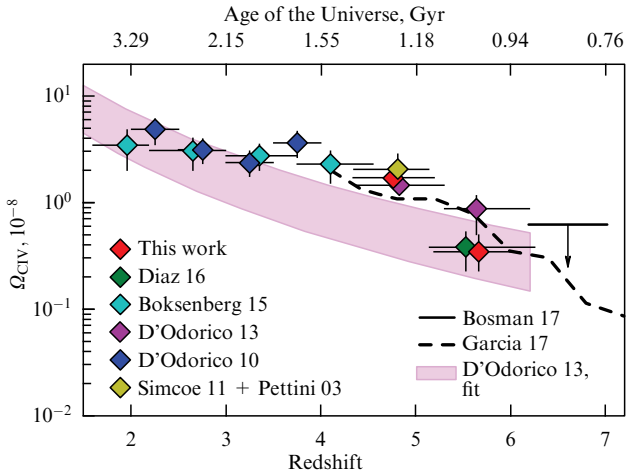

Figure 3. Mass fraction (in critical density units) of CIV ions in Lyα-forest (IGM) as a function of redshift. Observational data are presented in [143–147], as indicated in the legend; approximation (pink strip) is given in [145]. (Figure taken from [23].)

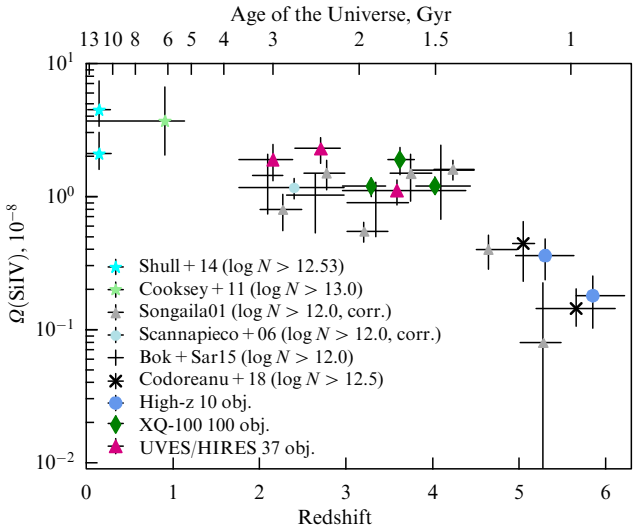

Figure 4. Mass fraction (in units of critical density) of SiIV ions as a function of redshift in the IGM plotted based on observations of SilV ion absorption lines. Observational data are presented in [23, 146, 148–150]; data for 37 objects in the UVEX/HIRES sample and 10 objects with redshifts $z \simeq 5-6$ are presented in [151] in Tables 1 and 3, respectively (see also Fig. 1 in [151]). (Figure taken from [151].)

4.1.1 Systems with saturated Lyα lines. The lines usually used for diagnostics are the hydrogen resonance lines Lyα ($\lambda = 121.6$ nm), Lyβ (102.5 nm), etc., and lines of heavy element ions CIV (155 nm), OVI (103 nm), SilV (140 nm), NV (124 nm), and several others. Such lines appear both in dense objects, observed as systems of Lyα lines with the column density $N(\mathrm{HI}) \geqslant 2 \times 10^{20}$ cm^{-2} (which are the DLA systems mentioned above), and in extended regions of intergalactic gas with the atomic hydrogen column density, $N(\mathrm{HI}) \leqslant 10^{17}$ cm^{-2}, Lyα forest lines [155].

The DLA systems apparently appear in the densest regions of gas associated with galaxies and their immediate environment (see, for example, [156]). This hypothesis is supported by recent measurements of a possible correlation between the metallicities of DLA systems and emission on the Lyα line excited presumably by a young stellar population associated with the region where absorption lines are formed [157, 158]. This interpretation is also in agreement with numerical models [159]. It may be asserted with some reservations that at $z > 4$ the DLA systems exhibit an evolutionary trend in $Z \propto (1+z)^{-0.2}$ metallicity, albeit with a large scatter, as can be seen in Fig. 5.

In later epochs, in the vicinity of the star formation peak at $z \sim 2.5-4$, the pattern is violated: the spread of metallicity for a fixed z reaches three orders of magnitude. The reasons for this spread are unclear. It seems apparent to associate it with the high SF rate, an order of magnitude greater than that in the modern era [137]. According to the authors of [158], such a scatter may be due to the DLA systems during this period being galactic disks filled with multiple isolated compact ISM regions with a high SF rate, which are over-enriched in metals due to intense supernova explosions. In later epochs, $z < 2$, the trend is restored.

4.1.2 Metals in the Lyα-forest and in 'voids.' The 'forest' of Lyα lines observed in the spectrum of quasars corresponds to absorption by neutral hydrogen in various regions of the

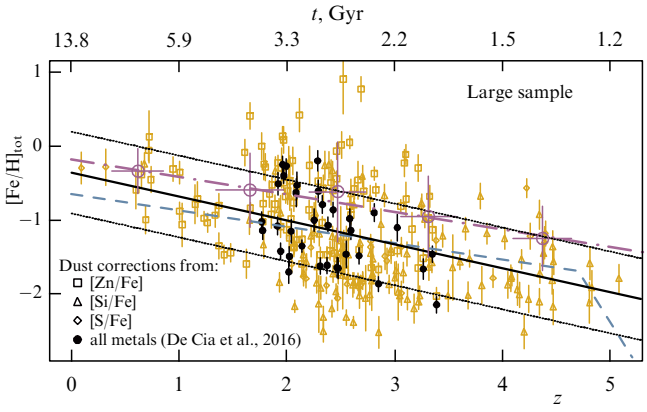

Figure 5. Evolution of metallicity in DLA systems. Symbols show ratios of elements on the basis of which observational data were adjusted (see text). Orange symbols represent a large sample [19], while black dots indicate early results with a limited sample [160] where metallicity was adjusted based on relative (with respect to iron) densities averaged over all observed elements. Black solid and dashed lines show a linear fit and variance over a large sample; blue broken line illustrates data from article [161]; large magenta circles show average metallicities 'weighted' using measured column densities of atomic hydrogen N(HI) in DLA systems. (Figure taken from [19].)

intergalactic medium, modulated by a large-scale structure. In this case, the strongest lines with the column densities $N(\mathrm{HI}) \sim 10^{17}$ cm^{-2} are formed in the walls of the structure, while the weakest, $N(\mathrm{HI}) \lesssim 10^{12}$ cm^{-2}, in cosmic voids, which are giant regions of intergalactic space with decreased density surrounded by thin 'walls' with increased density.[14]

Our modern understanding of the dynamics of structure formation in the Universe is largely based on numerical dynamic models, including a subgrid[15] description of stellar nucleosynthesis. The first models of this kind exhibited reliable agreement with the observed characteristics of the Lyα forest (see [164–171]). Recent progress in this approach makes it possible to distinguish and compare with observations subtler morphological features: nodes, filaments, walls, voids — with a mass accuracy of $\sim 10^7\, M_\odot$ [172–176].

Already the earliest identifications of metal absorption lines in the IGM showed a significant amount of metal up to redshifts $z \sim 3$: approximately half of the Lyα-forest systems with $N \geqslant 3 \times 10^{14}$ cm^{-2} and almost 100% of systems with $N \geqslant 10^{15}$ cm^{-2} feature absorption in the CIV doublet λ1548, λ1550 [177, 178]. Subsequent observations of the CIV and SiIV absorption lines at redshifts $z = 5.5$ showed the carbon abundance C/H $\sim 10^{-3.5}$ of the solar value, assuming that the fraction of triply ionized carbon[16] $x(\mathrm{CIV}) \sim 0.5$ [22].

Absorption lines of metals are visible in the spectra of the Lyα forest up to redshifts $z \sim 6$ [23, 145, 147, 153, 179–181]. The diagram displayed in Fig. 3 shows the evolution of the CIV ion density parameter in the range from $z \sim 6$ to $z \sim 2$; extrapolation extended it up to $z \approx 1.5$ [145]. It is of importance to emphasize that at redshift $z \simeq 6$ the CIV mass fraction is approximately half an order of magnitude smaller than that at $z \simeq 5.5$ [151, 153]. It can be easily seen that this value coincides with the epoch of complete reionization (see discussion in Section 3.1). Assuming the relative elemental composition in the IGM to be solar and the relative concentration of the CIV ion in the absorption regions x(CIV) to be ~ 0.3, we can estimate the average abundance of heavy elements in the IGM from $\zeta \sim 10^{-4}$ (at $z \simeq 5.5$) up to $\sim 10^{-3}$ (at $z \simeq 1.5$). It should be noted that the abundance of metals in the intergalactic medium is usually measured by the density parameter of the observed ions, as is done, for example, in Fig. 3. This is often associated with great uncertainty in the ionization state of the gas. Therefore, for example, the transition from the observed column density of the CIV ion to the abundance $\chi_\mathrm{C} = N(\mathrm{C})/N(\mathrm{H})$ requires knowledge of the ionization state of both carbon and hydrogen. Such knowledge is not always available, given uncertainties in gas density and ionizing radiation flux.

Metals are also present in regions with lower column density $N(\mathrm{HI}) < 1.4 \times 10^{13}$ cm^{-2} at $z \sim 3$ [182, 183] pertaining to cosmic voids with a baryon density an order of magnitude lower than the density in the walls (see [171, 184–186]). The space of a void with size $R \gtrsim 3-10$ Mpc[17] [187] over cosmological time ($t \sim 2 \times 10^9$ years in epoch $z \sim 3$) can be partially filled with emissions from galaxies localized in the walls. The active galaxies located in a relatively short-lived phase of a galactic 'hurricane' exhibit outflow velocities of $\sim 1000-3000$ km s^{-1} [188, 189]. However, when propagating in a homogeneous medium, the outflow velocity quickly decreases as $r^{-3/2}$. A recent analysis of the absorption in Lyα lines in voids close to us shows that the spatial distribution of the density of Lyα absorption is concentrated towards the void center [190]. Such a distribution can arise if the gas density decreases with distance from the walls as $\rho \propto R^{-2}$, so the shock wave velocity does not decrease. In addition, active galaxies in voids can enrich IGM *in situ*.

4.1.3 On the distribution of metals in the intergalactic medium. The fundamentally important issue of the spatial distribution of chemical elements in the IGM and the scale of its inevitable inhomogeneity has not been addressed for a long time. Numerical models indicate that the specific features of the mechanisms of matter mixing in IGM predetermine the extreme inhomogeneity of the distribution of metals [85, 86, 118, 119]. Moreover, those limited observational data on the distribution of chemical elements at redshifts $z = 3-6$, which span the era of the onset of massive stellar nucleosynthesis, show that the spatial distribution of heavy elements can indeed be highly inhomogeneous. In [191], a weak anti-correlation between the size and metallicity of the absorbing region of the Lyα forest, predicted in numerical models [85, 86], was revealed. As noted in [86], such anti-correlation is natural in all cases of metal transfer from small to large scales, regardless of the transfer mechanism. This effect can lead to observational selection that distinguishes metal-poor regions in the IGM. The discussion of this issue is continued below in Section 7.

Studying the spatial distribution of heavy elements in the IGM is an extremely challenging task. One of the reasons is

[14] Gas densities in the voids and in the walls are characterized by density contrast: $\delta(\mathbf{x}, t) = \rho(\mathbf{x}, t)/\bar{\rho}(t)$; voids correspond to $\delta(t) < 1$, and walls $\delta(t) > 1$; details are presented in reviews [162, 163].

[15] That is, a phenomenological description of physical processes based on simplified theoretical schemes on scales smaller than the resolution of the numerical grid.

[16] That is, $x(\mathrm{CIV}) = n(\mathrm{CIV})/n(\mathrm{C})$.

[17] 1 Megaparsec $= 3 \times 10^{24}$ cm.

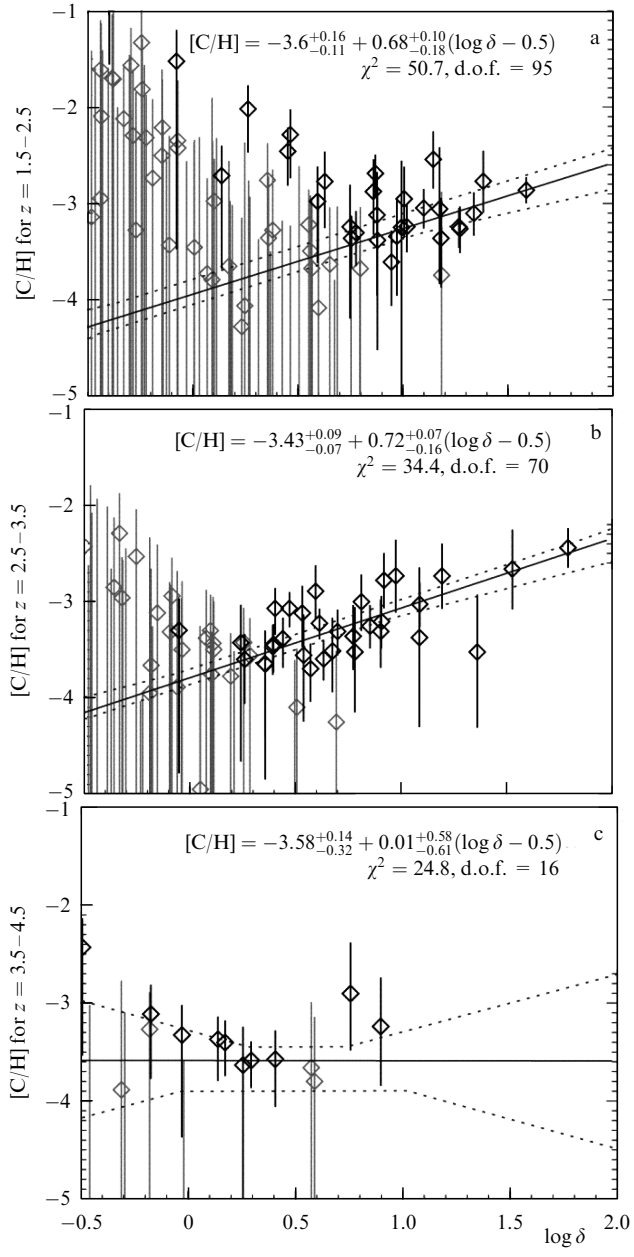

Figure 6. Carbon abundance in IGM as a function of density $\delta = \rho/\bar{\rho}$ according to measurements of absorption of the CIV ion. Shown from top to bottom are dependences of δ on density for redshifts indicated along the y-axis; gray symbols indicate data for which the lower error limit is $1\sigma = -\infty$. (Figure taken from [183].)

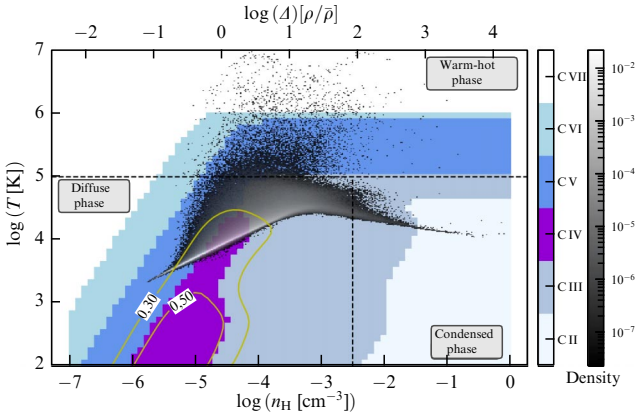

Figure 7. Distribution of carbon ionization state in the model of the intergalactic medium in epoch $z = 4.5$ on the $n-T$ plane obtained by cosmological modeling. Color palette indicates areas corresponding to the dominance of a particular carbon ion. (Figure taken from [194].)

that the analysis of absorption lines yields the concentration of ions of a particular element in the line of sight $N(X)$ [cm^{-2}] and the corresponding concentration of hydrogen atoms N(HI) [cm^{-2}]. However, data on the volume density of absorbing regions and, generally speaking, their spatial distribution are unavailable and can only be determined indirectly, usually in hybrid approaches using observations and numerical experiments. An example of such an approach is presented in [183], where the results of numerical modeling of structure formation and ionization equilibrium in the intergalactic medium were fitted to observations using the χ^2 method. This approach made it possible to relate the observed column densities of the CIV ion (N(CIV)) to the local contrast δ in the absorbing region. It seems apparent that areas with higher relative density δ should correspond to higher values of column densities. For atomic hydrogen, such a relation has a simple form [192]:

$$\delta \simeq 10\left(\frac{N_{\rm HI}}{10^{15}\ {\rm cm}^{-2}}\right)^{2/3}\left[\frac{(1+z)}{4}\right]^{-3}, \qquad (1)$$

i.e., smaller δ correspond to regions of rarefied IGM gas, while larger δ, to regions near galaxies and their clusters-to-be. The behavior of N(CIV) with increasing δ is not this straightforward: there is a certain density value, which depends on the flux of ionizing UV radiation, at which the relative concentration of CIV ions decreases due to recombination. However, in any case, the lowest column densities N(CIV) definitely correspond to the most rarefied IGM regions with $\delta < 1$.

Figure 6 shows the dependence of the relative carbon abundance $[{\rm C/H}] = \lg({\rm C/H}) - \lg({\rm C/H})_\odot$ on the density of absorbing gas δ. At the early stages, $z = 3.5-4.5$, the metallicity in a wide interval of densities ranges primarily between -3.5 and -3.0. In the epochs close to us, metallicity generally increases, especially in the interval $z = 1.5-2.5$, which corresponds to the peak of star formation in the Universe. At the same time, the dispersion of metallicity also increases, especially in regions of cosmic voids with low density $\lg\delta < 0$. Thus, during the transport of heavy elements from circumgalactic space into the intergalactic medium, and especially in the region of cosmic 'voids,' matter turns out to be increasingly less mixed.

This pattern, however, can be complicated by the fact that at low densities the characteristic times for establishing ionization equilibrium in processes associated with recombination or collisional ionization are large, so the ionization state can turn out to be strongly dependent on the thermodynamic history of the gas [193]. The carbon ionization state in the IGM under the assumption of *stationary* photoionization by the intergalactic UV radiation field was determined in more detail in the cosmological model of enrichment and ionization [197]. Figure 7 shows a diagram of the ionization state of carbon on the $n-T$ plane for IGM gas obtained in this model. It illustrates well the importance of the knowledge of the IGM gas ionization state for confident interpretation of the observed CIV characteristics.

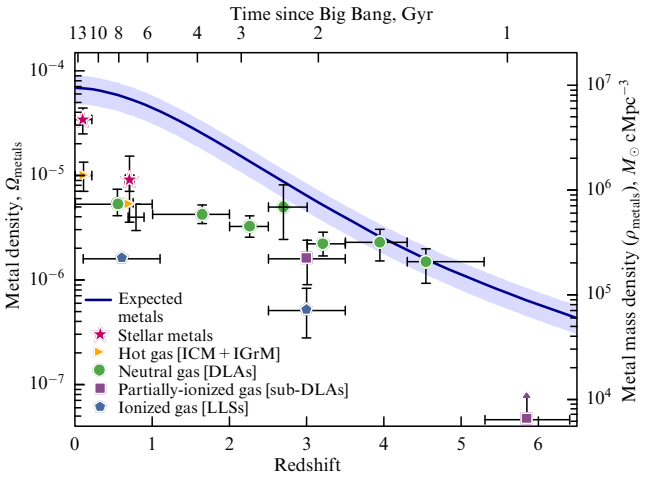

Figure 8. Evolution of the total average mass of metals per unit of comoving volume of the Universe. Solid curve with an uncertainty band shows the expected metal density $\rho_Z(z)$ estimated using the measured SF rate $\dot{\rho}_*(z)$. (Figure taken from [207].)

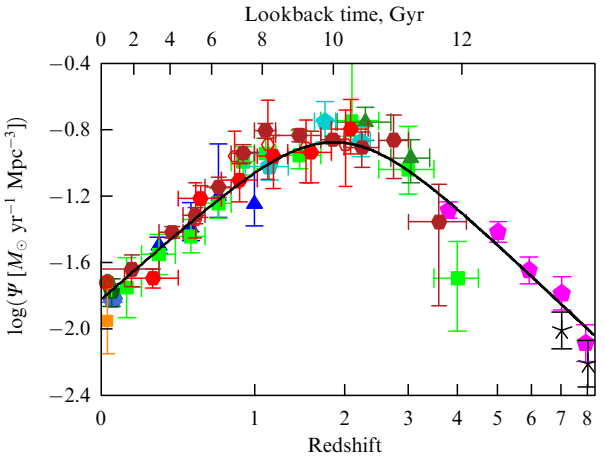

Figure 9. History of star formation in the Universe constructed based on the measurements of emission in the far ultraviolet (FUV) and infrared (IR) ranges in the rest frame. (Figure taken from review [137].)

4.1.4 Metals in the galaxy cluster gas. Another aspect of the redistribution of metals in the Universe on large scales relates to the hot ($T \sim 10^7 - 10^8$ K) gas of galaxy clusters (ICM). Due to a high temperature and low density ($n \sim 10^{-3}$ cm^{-3}), the gas in the clusters is highly ionized, so the determination of metallicity in it is based on measurements of the heavy-element emission lines in the X-ray region of the spectrum. The brightest of them is the so-called 'iron K-line,' which is a blend (superposition) of close lines of multiply charged Fe^{+24} and Fe^{+25} ions and a nickel ion with an energy $\simeq 6.5-7$ keV [195–199]. A detailed discussion can be found in reviews [200–203]. Despite the apparent similarity with the problem of enrichment of the intergalactic medium, the enrichment of gas in galaxy clusters is fundamentally different from a dynamic point of view due to the denser environment, frequent tidal interactions among galaxies, and the resulting surges of star formation on short spatial and temporal scales, a consequence of which is a significantly higher metallicity in the gas of clusters $Z \sim 0.3 Z_\odot$ [25, 200, 204, 205]. Under such conditions, relics of the initial enrichment in the galaxy cluster gas are lost. We note in this regard that recent studies of gas metallicity in several groups of galaxies in their outer ($R > 0.25 R_{200}$) regions have revealed a surprising similarity between the spatial distribution and metallicity value determined for iron, $Z_{\rm Fe} \simeq 0.309\, Z_\odot$, and those of their counterparts in large clusters [18] [206].

4.2 Budget of metal in the Universe

Based on Fig. 5, we can conclude that both in the modern epoch $z \lesssim 0.15$ and in galaxies represented by DLA systems, cold gas contains a significant portion of the metals produced in the Universe. This is indicated by the fact that at $z \to 0$ the metallicity is $\zeta \to 0.5$ ([Fe/H] ≈ -0.3). According to calculations [207], most of the missing metals are associated with stars. Simple estimates show that in the post-reionization epoch $z \approx 4-5.5$, metals were also concentrated primarily in the cold gas of young galaxies. However, in the redshift range near the star formation peak $z = 2-3$, and after it at $z \approx 0.5-2$, a significant deficiency of metals compared to the expected one is detected, as shown in Fig. 8. In the figure, the symbols show estimates of the metal density parameter based on direct observations, and the solid line represents the theoretical estimate of the mass of metals, obtained on the basis of an independent observational evaluation of the star formation rate in the Universe $\dot{\rho}_*(z) = \Psi(z)$, shown in Fig. 9. Knowing the SF rate, it is possible to find the metal production rate $\rho_g \dot{Z} = y(1-R)\Psi$, where $y \simeq 0.033$ is the mass fraction of metals averaged over the IMF [137, 208], and Ψ, R is the fraction of mass returned to the ISM by the stellar wind and supernovae [137, 207, 209].

The mass of metals produced by time $t(z)$ is

$$\Omega_Z(z) = y \rho_{\rm cr}^{-1} \int_{t(z)}^{t(\infty)} \Psi(z) \left| \frac{{\rm d}z}{{\rm d}t} \right| {\rm d}t\,. \qquad (2)$$

The result of integration is shown as a solid curve. A clear deficiency of metals compared to the theoretical prediction is seen in the region between the SF peak $z \sim 2-3$ and $z \lesssim 0.15$. The paper [207] estimates that at $z \approx 1.5$ the deficit is 83% (see also Fig. 9 in [207]).

The problem of 'missing' metals was first brought to the fore more than 20 years ago in [210]. Subsequently, many authors repeatedly returned to it with a discussion of potential reservoirs. The most plausible hypothesis seems to be one in which the missing mass of metals can be contained in the so-called 'warm-hot' phase [19] of the IGM with a gas temperature of $T \sim 10^5 - 10^7$ K. The existence of a 'warm-hot' phase is associated with the action of strong shock waves in the region of Lagrangian singularities during the formation of the large-scale structure [211, 212]. It is hypothesized that at such temperatures the gas is highly ionized and therefore it is invisible in absorption, and its observation in emission in the optical and ultraviolet regions of the spectrum is strongly hindered. Numerical models predict that the mass fraction of metals in the 'warm-hot' phase of the IGM is up to 50% [212–215], although such estimates often turn out to be highly model dependent [216]. Direct observations are not yet sufficient to confidently identify WHIM as the main reservoir of missing metals. Recently, reports have appeared on the detection in the X-ray region of the absorption line of

[18] This option was brought to our attention by a reviewer.

[19] WHIM (Warm-Hot Ionized Medium).

the multiply charged OVII ion, which supposedly emerged in the WHIM layer [217].

Among other factors that can lead to the 'loss' of metals are numerous effects of observational selection (a detailed discussion of the aspects of their influence on the calculation of the mass of metals is presented in [216]), which are direct errors in observational estimates of the mass of metals due to the above-mentioned uncertainties in the ionization state of the gas and insufficient resolution in numerical models of the chemical evolution of the Universe [218]. One of the important and unavoidable reasons that a 'loss' of metals can arise is the very process of transfer of metals from a 'point' source — the burst of an individual supernova, a star cluster with a size of no more than a few parsecs — to significantly larger scales of tens and hundreds of kiloparsecs. It is natural to expect that under such conditions, during the transfer process, the metallicity Z turns out to be a decreasing function of the distance from the source $Z \propto r^{-\alpha}$. Therefore, in conducting observations in absorption lines, the probability that the line of sight from a radiation source (quasar) passes through a region with metallicity Z drops as $P(Z) \propto Z^{-2/\alpha}$ [86]. A discussion of these aspects is continued in Sections 7.3 and 7.4.

5. Mechanisms of metal ejection from galaxies

The mechanisms of matter exchange between the IGM and galaxies can be divided into two groups according to the 'direction of influence': galaxy to IGM and IGM to galaxy. The first group includes the ejection of matter from galaxies due to supernova explosions, radiation pressure, tidal interaction of galaxies, and stripping of the gas component off the galaxy under the influence of dynamic gas pressure IGM (ram stripping). The second group includes the accretion of chemically distinct IGM matter in the galaxy, the most important element of its interaction with the IGM which maintains its growth and 'life activity.' In this review, we only consider mechanisms of the first group.

5.1 Shock waves from supernovae

The ejection of matter from galaxies is associated with the energy release of massive stars, which includes shock waves from supernovae and the pressure of stellar radiation on matter. In numerical calculations on scales exceeding galactic ones, it is usually assumed that the rate of gas outflow from galaxies $\dot{M}$ is proportional to the star formation rate $\dot{M}_*$ or, equivalently, to the frequency of supernova bursts $\nu_{\rm sn}$. Given the nonlinear nature of many of the phenomena involved, this assumption is fairly bold. Nevertheless, it works, since observations show that the rate of gas mass loss by galaxies[20] is $\dot{M} \sim 0.3-30\,\dot{M}_*$ [219–222].

The ejection of matter by supernovae is based on the 'breakthrough of the atmosphere' effect, first described by A S Kompaneets [223]. A shock wave in an inhomogeneous (stratified) medium propagates predominantly in the direction opposite to the density gradient $v \simeq \sqrt{P_{\rm s}/\rho(z)}$, where $P_{\rm s}$ is the pressure behind the SW front. Therefore, in the case of a limited stratified medium, an exit of a SW beyond its limits, an outburst, is possible if the time $t_{\rm b} \propto \int^{\infty} v^{-1}\,{\rm d}z$ is finite; here, the integration is carried out in the direction opposite to the density gradient. The integral is finite in media with a fairly steep density profile, for example, in exponential $\rho \propto \exp(-z)$ media. In the simplest case of an expanding shell from a point source with constant power, the polar regions of the expanding shell only carry from 5% to 10% of the shell mass outside the interstellar gas disk [224], while most of the matter in its walls is entrained downward by gravity. This yields $\dot{M} \sim 5-10\dot{M}_*$.

5.1.1 Ejections from dwarf galaxies. Low-mass galaxies make the predominant contribution to the enrichment of the Universe with metals. This is due to the following factors: (1) the binding energy of such galaxies is lower, and therefore lower values of energy release can result in a breakthrough of the interstellar gas layer; (2) weaker requirements for energy release enable the ejection due to the burst of only a few supernovae in more numerous low-mass star clusters $\phi(m) \propto m^{-1}$; (3) low-mass galaxies numerically dominate more massive galaxies, as follows from the Press – Schechter law ${\rm d}N/{\rm d}\ln M \propto M^{-0.9}$.

For a point source with mechanical power L located in the ISM disk plane, a breakthrough of the disk and ejection of matter outside the galaxy are possible provided [74, 119]

$$L > \xi \rho_{\rm d} H^2 \left(\frac{GM_h}{r_h}\right)^{3/2}, \tag{3}$$

where $\xi \sim 1$ is a dimensionless factor characterizing the features of gas outflow during ejection, $\rho_{\rm d}$ is the average density of the gas disk, H is the height scale of the gas disk, M_h is the total mass of the galaxy, including baryonic and dark matter, and r_h is the corresponding radius. For a galaxy with a mass of $M_h \sim 10^{11}\,M_\odot$, $r_h \sim 10$ kpc, an outflow velocity of $v_{\rm e} \sim \sqrt{2GM_h/r_h} \sim 100$ km s^{-1}, and a gas height scale of $H \sim 100$ pc, the power required for a breakthrough is $L \sim 1.5 \times 10^{39} n_{\rm d}$ erg s^{-1}, where $n_{\rm d}$ is the density of particles in the gas disk. This set corresponds to a fairly modest SF rate of $\dot{M}_* \sim 0.006\,M_\odot$ per year. The estimated mass loss rate for such galaxies is

$$\dot{M} \sim \xi_{\rm esc}\,\frac{2L}{v_{\rm e}^2} \sim 10\xi_{\rm esc}\dot{M}_*\,. \tag{4}$$

Here, $\xi_{\rm esc} \sim \Delta\Omega/4\pi$ is the fraction of the mass involved in the outflow that has gone beyond the galaxy, and $\Delta\Omega$ is the solid angle of outflow collimation. For an outflow generated by a star cluster, $\xi_{\rm esc} \sim 0.01$ [224, 225]; for coherent SF bursts in the centers of galaxies, where the flow extends far beyond the thin ISM disk, $\xi_{\rm esc}$ can reach a value of $\sim 0.1-0.3$, depending on L [226].

At large redshifts, where the IGM density is greater, the IGM pressure is significant. This can be seen from a simple estimate of the maximum radius of the shock wave $R_{\rm s} \sim (\dot{M}v_{\rm e}/P_{\rm IGM})^{1/2} \propto (1+z)^{-3/2}$, where $P_{\rm IGM}$ is the pressure of the surrounding IGM gas [119]. As a result, the filling factor of metal-enriched regions decreases: cosmological numerical models yield a volume filling factor $Q_{\rm V} \sim 0.01(1+z)^{-1}$ for regions with metallicity $Z \approx 10^{-3}-10^{-2}$ and values 2 to 2.5 orders of magnitude smaller for the areas with $Z \approx 0.1$ [152]. Moreover, the surface factor, i.e., the probability of crossing a line of sight of length ℓ, is of the order of $Q_{\rm S} \sim Q_{\rm V}\ell/R_{\rm s}$, so enriched regions can be detected at cosmological distances. A more detailed discussion of these aspects can be found in [138, 152, 227–233].

5.1.2 Ejections from massive galaxies. The ejection of matter by supernovae from massive galaxies requires noticeably

[20] The ratio $\eta_m = \dot{M}/\dot{M}_*$ is referred to as mass loading outflow.

greater supernova power. In this case, the most significant factor determining the efficiency of the ejection of matter by shock waves from supernovae is the coherence of bursts (i.e., a high frequency of bursts within a relatively small region of the galaxy) [119, 234–236]. A regime close to coherent is achieved in young star clusters (OB associations), where supernovae explode in a compact region on a relatively short time scale, i.e., in a fairly synchronized way. Only those collective bursts whose total power exceeds the threshold value L_c, which depends on the galaxy's mass and morphological type [224, 225, 234–241], result in a breakthrough of the interstellar disk. In our Galaxy, the number of such OB associations, the power of which is sufficient to form gas emissions in the IGM, is about 60 [242]. This value is consistent with the number of vertical gas structures (worms) in the Galaxy observed on the 21-cm line of neutral hydrogen, which are presumably dense walls of the outflows due to supernova explosions [243–245].

As the mass of the galaxy increases, the critical mechanical luminosity increases faster than the maximum luminosity of the OB association with a limited number of stars. Under these conditions, only the most massive OB associations can eject mass from the galaxy [230, 246–250]. Therefore, the efficiency of ejecting the interstellar gas mass into the intergalactic medium decreases with increasing mass of the galaxy.

Central powerful star formation bursts, which are observed, for example, in the galaxies M82, NGC3079, NGC1482, etc., can lead to the ejection of mass outside the galaxy and, possibly, into the intergalactic medium. General considerations suggest that such galaxies 'participate' in the chemical evolution of the Universe, but any reliable assessment of their contribution is currently difficult, inter alia, due to significant uncertainty in estimates of the periodicity of star formation bursts, the mass loss rate, the fraction of mass reaching intergalactic space, metallicity of the ejected substance, etc. [219, 251, 252]. For example, a detailed analysis of the M82 galaxy closest to us with a powerful galactic wind shows that the amount of matter ejected from the central region decreases very rapidly with distance from the center. The brightness of the image on the 21-cm line of atomic hydrogen falls approximately according to the law $\sim r^{-2}$, where r is the distance from the center of the galaxy, and this can be interpreted as an outflow into the IGM. However, the IR emission profile of cold dust and gas on the CO-molecule lines, diminishing as $\sim r^{-3}$, indicates that the flow does not go beyond the galaxy's boundaries [251]. In this sense, the problem of mass 'entrainment' and the apparent disagreement between theoretical predictions and observations are actually the problem of measuring the outflow characteristics at large distances from the source galaxy.

5.1.3 Circumgalactic halos. In the last decade, in relation to the problem of the 'transport' of metals from supernovae to scales of several Mpc (i.e., into a space, the dimensions of which are five orders of magnitude larger than those of the source), structures of intermediate scales ranging from ~ 30 kpc to ~ 300 kpc have been discussed. These structures are the circumgalactic halos discovered and described in [24]. We are considering giant gas coronas around galaxies ranging in size from 100 to 300 kpc and sometimes more, filled with hot gas with a high number density of heavy elements. Gas in such extended halos flows out at velocities that, with rare exceptions, are close to ~ 100 km s^{-1}, a value which is

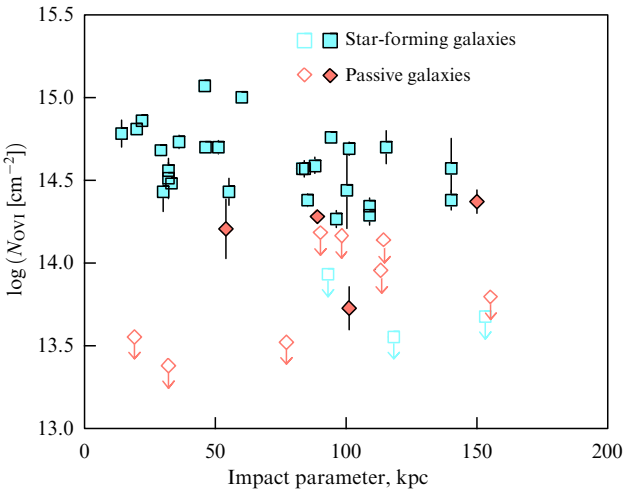

Figure 10. Line-of-sight (projected) profile of the distribution of OVI ions in circumgalactic halos discovered in the COS-halo survey [24]. See details in the text.

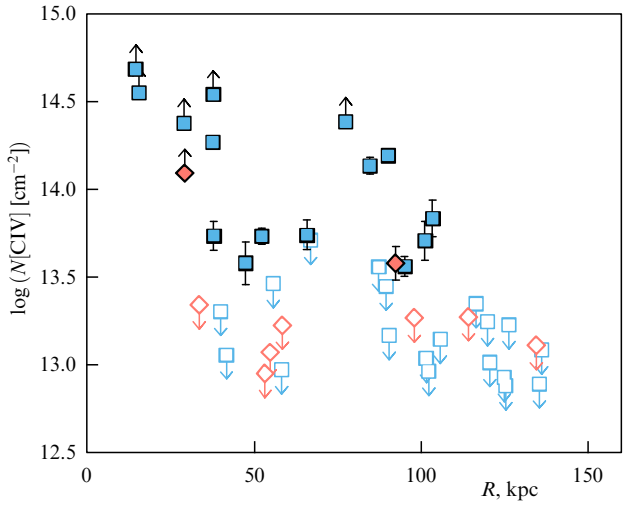

Figure 11. Distribution of CIV ions in the halo discovered in the COS-dwarfs survey [253]. See details in the text.

significantly less than the escape velocity; therefore, halos are formed as a result of a relatively slow outflow on a time scale of 1 Gyr.

Figure 10 shows the 'average' radial profile of the OVI ion distribution obtained from measurements of the distant neighborhoods of 42 galaxies from the COS-halo survey.[21] Light blue squares show the number densities for galaxies with active star formation (SF rate $\dot{M}_\star \sim 1\, M_\odot$ per year), and orange squares represent passive galaxies with an SF rate an order of magnitude lower [24]. This was followed by observations of such extended halos in dwarf galaxies (see the survey of COS-dwarfs [253]). Figure 11 shows the radial profiles of the CIV ion in some galaxies. As can be seen, metal-enriched gas coronas extend in this case to comparable scales of ~ 100 kpc, despite the smaller masses of the galaxies.

A conclusion of importance for the problem of IGM enrichment in metals is that such extended gas coronas around galaxies perform as a dynamically complex interface between galactic disks and intergalactic gas, filled with counter flows that ensure the galaxy's life activity.

[21] COS (Cosmic Origin Spectrograph/Hubble Space Telescope).

The downward (accretion) flow brings 'fresh' gas into galaxies from the intergalactic reservoir and supplies material for the formation of stars in galaxies, while the upward flow (outflow) removes processed metal-enriched matter from galaxies in a reverse 'cascade' chain from microscales of the order of several parsecs to intergalactic space megascales [254–256]. In general, circumgalactic halos may contain up to 50% of the baryonic mass of galaxies [257, 258], which manifests itself in Lyα-forest lines [259], although a more reliable estimate requires a detailed analysis of the physical state of the gas [260]. Currently, there is no understanding of the details of the complex dynamics of the interaction between these flows. Some aspects are discussed in Section 6.2 and in reviews [261–263].

5.2 Ejection of metals by radiation pressure

For a typical value of the energy density of the average interstellar radiation field, $\epsilon_{\rm uv} \sim 0.1-1$ eV cm^{-3}, the momentum flux carried by photons (and transferred to matter when scattered by dust particles) is only slightly less than that associated with shock waves from supernovae. This implies that radiation pressure can significantly affect the dynamics of interstellar gas and, in particular, can be responsible for its ejection from the galaxy. Taking into account that the above value of the momentum is related to the *average* radiation field, there is no need for coherency, i.e., synchronization of energy release episodes on short temporal and small spatial scales. The idea that radiation pressure is capable of maintaining gas in the galactic halo was first proposed in [264–266]. Moreover, it was shown in [266–268] that the pressure of the interstellar radiation field can accelerate dust grains to high speeds and eject them far beyond the Galaxy, into intergalactic space on time scales of $\sim (0.03-3)a^{-1}$ Gyr, depending on the size of the dust grain a [269].

The criterion for the occurrence of wind under the influence of radiation pressure is $\kappa I/2\pi\tilde{c}G\Sigma \gtrsim 3$, where κ is the opacity coefficient, Σ is the surface density of the stellar disk, I is the surface brightness of the disk radiation, and $\tilde{c} \sim 10$ is the concentration parameter for the Navarro–Frank–White profile [268]. Since the radiation energy density is distributed more diffusely than the shock wave density, radiation pressure is of greater importance in massive galaxies [270, 271].

The galactic interstellar magnetic field $B \sim 10^{-5}$ G [272] significantly alters the picture. The typical value of the cyclotron radius for a dust particle[22] in the interstellar medium is only $R_{\rm G} \sim 0.03$ pc, i.e., dust particles are actually 'glued' to magnetic field lines (R-J Dettmar and Yu A Shchekinov, private communication (2011)). Therefore, transport in the vertical direction is only possible in the form of 'channeling' along the vertical magnetic field, if any. In some edge-on galaxies, a vertical magnetic field is observed in their halo [274–276]. Due to insufficient angular resolution, it is currently difficult to estimate the fraction of such galaxies. From a theoretical point of view, the generation of a significant vertical component B_z is quite possible under the effect of a spherical turbulent dynamo in the halo [277, 278] and as a result of the development of Parker instability [279]. In the latter case, even one supernova may be sufficient to trigger the Parker instability with the formation of magnetic loops extending far beyond the disk, up to $z \sim 4-5$ kpc [280]. Moreover, calculations show that the inflationary growth of the Parker loop continues formally without limits, i.e., beyond the calculation area of 32 height scales [281]. Under such conditions, the assumptions of [266, 267] are fulfilled, and, therefore, if the fraction of the galactic disk surface occupied by magnetic fields extending into intergalactic space is sufficiently large (about 0.1), the loss of dust mass by the galaxy can be significant: according to estimates made in [266], for our Galaxy, this value may be of the order of $0.04\,M_\odot$ yr^{-1}, which is 10% of the rate of metal production in stars.

However, it should be emphasized that, despite the apparent simplicity of the problem, a complete study of the dynamics of the gas-dust ISM under the effect of radiation pressure is extremely complicated consuming and is still far from resolved. This is due to the strong sensitivity of the dynamics to the parameters of the problem, including the dependence of the radiation scattering cross sections on the ratio of the wavelength to the particle size, the dependence of the friction force of dust grains in the surrounding plasma on the dust grain charge, the dependence of the dust grain charge on the spectrum of the radiation accelerating the grains and the parameters of the plasma in the immediate environment, etc. (see, for example, [267, 269, 282]).

When entering the intergalactic medium with a gas density $n \sim 10^{-6}$ cm^{-3}, a typical dust grain with a radius of 0.1 μm and matter density $\rho_{\rm d} \sim 3$ g cm^{-3} features the mean free path between collisions with an atom or ion of the intergalactic medium $\ell \sim 10^{16}$ cm and average deceleration length $L \sim (100-200)v_{\rm d,\,100}^2$ kpc, where $v_{\rm d,\,100}$ is the speed of the dust particle in 100 km s^{-1} units. The actual deceleration length of a dust particle is less than this value, since, when moving in the intergalactic medium and colliding with gas particles, and being under the influence of an external radiation field, the dust particle loses its mass and is decelerated more effectively. It is of importance that such destruction results in the transition of heavy elements from the condensed phase to the gas phase, and thus in the enrichment of intergalactic gas with metals [267].

An analysis of the transport of dust particles ejected from galaxies under the effect of radiation pressure, which was carried out in [267], shows that only large particles ($a > 0.1$ μm) can travel beyond 100 kpc around the parent galaxy and reach rarefied regions (with the density contrast $\delta \sim 1$) of the cosmic structure. Dust particles are subject to the strongest destruction due to collisions with the surrounding gas in dense regions with $\delta = 10-100$, where the collisions lead to the maximum loss of metals. Metals in the intergalactic medium are distributed in this scenario in an extremely inhomogeneous way, with a volume filling factor of about 10%. However, this conclusion is based on large-scale cosmological models with low spatial resolution ($\simeq 82h^{-1}$ kpc in comoving coordinate systems) with a subgrid description of physics at smaller scales. Even more recent approaches with a better resolution ($\gtrsim 1$ kpc) and a simple bimodal size distribution of dust particles only enable the dynamics of dust in the vicinity of galaxies and their halos to be assessed in general terms [283].

5.3 Tidal interactions of galaxies

The formation of an ensemble of galaxies in the early Universe via frequent approaches and hierarchical mergers is a powerful source of large-scale tidal movements capable,

[22] The charge of a dust particle with radius $a = 0.1$ μm in the diffuse interstellar medium is $Z_{\rm d} \sim +(45-255)e$ [273]. For dust grains of smaller radius, the charge-to-mass ratio is larger.

in principle, of transferring matter enriched in galaxies into the intergalactic medium on a scale of hundreds of kiloparsecs or more. The first models of enrichment in tidal interactions implemented on a coarse grid [284, 285] showed that the spatial redistribution of metals caused by tides turns out to be extremely inhomogeneous: metallicity varies from $Z \sim 10^{-5}$ to ~ 1 when passing from regions with density contrast $\delta \sim 0.1$ to regions with $\delta \sim 10^3 - 10^4$, corresponding to the transition from regions of intergalactic gas in cosmic voids to interstellar gas in galaxies. In other words, metals remain predominantly in the vicinity of their sources, i.e., galaxies. This result illustrates the insufficiency of a numerical resolution of $\Delta x \geqslant 0.1$ Mpc for modeling the phenomena of metal transfer from ISM disks with a characteristic density stratification scale of ~ 100 pc. Rough numerical grids are not sufficient to trace the collimated release of shock waves and metal-enriched matter from SN beyond the galaxy's limits due to the effect of breakthrough of interstellar disks [224, 225, 237, 286], especially for central bursts in galaxies [230, 287].

A scenario for the combined action of tidal forces and the energy release of massive stars in the transport of metals into the IGM was proposed in [119]. In this scenario, the transfer, which resembles a turbulent diffusion process, turns out to be more efficient. These two mechanisms operate on different scales: the former is effective on scales $0.01 \lesssim l_{\rm sn} \lesssim 10$ kpc, while the latter is operative on scales $10 < l_{\rm tid} \lesssim 50$ kpc. Tides propagate the action of the galactic wind, localized within the maximum radius of the galactic wind $R_{\rm s}(z)$ (see Section 5.1.1), expanding it to intergalactic scales. This conclusion was subsequently confirmed by numerical experiments: the combined action of tides and the galactic wind increases the volume filling factor of enriched matter in the IGM to a value of 0.35 [288]. It should, however, be taken into account that, due to inevitable limitations on the spatial resolution of numerical experiments, mass ejection in both tidal interactions and the galactic wind is described in a phenomenological way without a detailed study of the dynamics on galactic and subgalactic scales (see a discussion in Section 5).

6. Numerical description of enrichment

6.1 Phenomenological experiments

Phenomenological numerical experiments are understood as experiments based on 'cosmological' codes that describe the dynamics of large regions of the Universe on scales of ~ 100 Mpc, including the formation and dynamics of galaxies and their clusters (see, for example, [162, 289, 290]). The standard numerical resolution corresponds to a baryon mass in a cell of $\sim 10^6\, M_\odot$. Therefore, in problems related to galaxy formation, their demography, and the exchange of matter on intergalactic scales, this translates into a spatial resolution of $\Delta x \sim 60$ kpc in the comoving system. In problems related to phenomena in the ISM of galaxies, for a typical ISM density, this implies a cell size of ~ 300 pc. In certain selected regions of the computational domain, adaptive grids are used with cells sized to 10–30 pc, which makes it possible to resolve some details of the object being formed. A number of problems associated with physical processes on subparsec scales, which include problems of metal redistribution in the Universe, cannot yet be solved with cosmological codes and can so far only be explored using subgrid 'prescriptions' [162, 263]. Until recently, in global

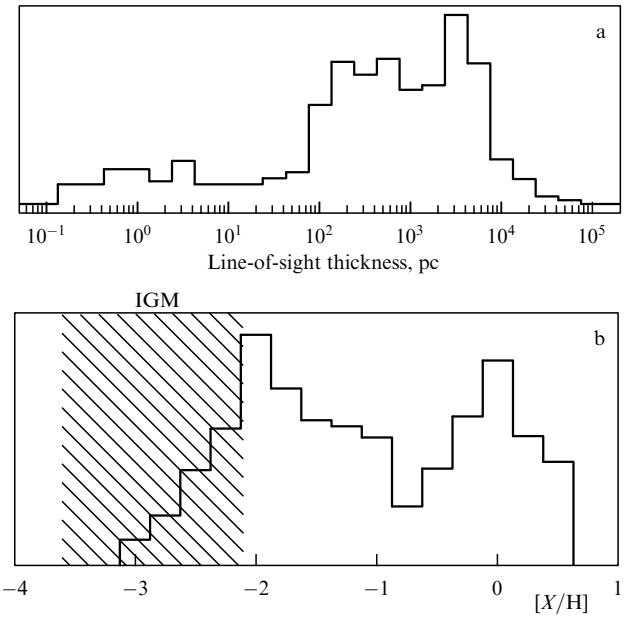

Figure 12. (a) Size distribution of absorbing clouds along the line of sight, (b) metallicity distribution. (Figure taken from [294].)

'cosmological' numerical schemes, both the sources of metals and their distribution on large scales remained deep 'below the grid' by 2 to 3 orders of magnitude [152, 291–293].

The need for numerical modeling of the 'micro-level' processes hidden 'beneath the grid' is well illustrated by direct observations of the distribution of density and metallicity in the intergalactic space at $z \sim 2.3$ in [294]: in a volume with a comoving radius $\geqslant 1$ Mpc, a population of enriched gas condensates with line-of-sight sizes ranging from ~ 0.1 pc to $\lesssim 100$ kpc was discovered. The metallicity of the gas in the condensate varies from $Z \lesssim 10^{-3}\, Z_\odot$ to $Z \gtrsim 3\, Z_\odot$; the upper limit presumably represents fragments of an unmixed supernova shell. The gas density in the condensates ranges from $n \gtrsim 10^{-4}$ cm^{-3}, a value two orders of magnitude larger than the intergalactic density at $z \simeq 2.3$, to $n \lesssim 0.1$ cm^{-3}; the ratio of median gas density and the IGM density is $\rho/\rho_{\rm IGM} \sim 100$ [294] (Fig. 12). Therefore, the dynamic scale of numerical modeling that spans 4 to 5 orders of magnitude should necessarily encompass the entire grid and the entire time interval.

A weak element in phenomenological models is the assumption that galaxies lose mass proportional to the star formation rate. This assumption can be used with reservations for galaxies with bursts of star formation in the central region with radius $R \lesssim 0.5$ kpc. Under such conditions, frequent supernova explosions cause the overlap of their remnants in the early stages of expansion, when energy losses are still small and their effect turns out to be cumulative ('coherent') with an effective mechanical luminosity of $L \sim E_0 \nu_{\rm sn}$, where $E_0 \sim 10^{51}$ erg is the energy of a supernova and $\nu_{\rm sn}$ is the frequency of bursts in the central part of the galaxy [235]. In galaxies with quiescent SF, supernova explosions are distributed over the galactic disk with radius $R \sim 10$ kpc, and their effect on the surrounding interstellar gas turns out to be unsynchronized. As a result, for the same total SF rate, outflows from galaxies with SF spread over the disk turn out to be weak. This is manifested in a decrease in the fraction of emitted matter with increasing

mass of the galaxies, as is confirmed by numerical experiments [234].

This is also evident in observations: only galaxies with central surges of star formation, such as M82, generate powerful outflows [219]. Galaxies in the quiescent SF regime with a sufficiently high star formation rate are not capable of forming outflows, but form extended gas halos with a height of several (3–5) kiloparsecs. In some cases, the possible existence of outflows from galactic disks into a halo is suggested by observations of filamentary vertical structures [295]; however, direct observations of the outflow of matter from an extended gas halo into an IGM are extremely rare. The detection of giant (with a radius exceeding 150 kpc) gas halos around distant ($z = 0.1-0.36$) galaxies, abundantly filled with heavy elements with $\zeta \simeq 1$ [24] (see Section 5.1.3), can be an indirect indication of the existence of such outflows.

In an even more pronounced form, the problem of maintaining large-scale outflows arises in modeling the transfer of heavy elements to scales spanning cosmic voids. Enrichment of voids with collimated outflows from galaxies localized in the walls requires high mechanical power of the central source $L \sim 3 \times 10^{41}$ erg s^{-1} for times of at least several billion years, as shown by phenomenological numerical models [122]. Moreover, even under favorable assumptions, such outflows can only enrich high-density regions, i.e., the walls of the cosmic structure in which galaxies are concentrated. It is possible that voids are enriched by galaxies *in situ*.

In the scenarios of galactic outflows driven by momentum transfer from radiation, the requirements for synchronizing stellar evolution are relaxed due to a more diffuse distribution of radiation in the ISM. As noted above in Section 5.2, even quiescent (without bursts) star formation can generate an amount of radiation sufficient to eject interstellar gas into the surrounding space. In its simplest form, the dynamics of suchlike models, where the interstellar gas outflow occurs due to the transfer of momentum from radiation to interstellar dust grains and further to the gas component, were formulated in [265, 266] and in [267] in close connection with the problem of enriching the Universe with metals.

Therefore, a significant limitation of phenomenological models is that they can only provide the Universe's metallicity averaged over large volumes, while the parameters of the spatial distribution of metals in the intergalactic medium remain largely uncertain. Taking into account the expected low values of the volume filling factor of enriched intergalactic matter [152], the spatial features of the metallicity distribution in the IGM discovered in [294] are still unresolved. For this reason, it cannot be ruled out that some part of the predicted correlations and patterns is directly determined by subgrid 'prescriptions.'

6.2 Dynamic experiments

Dynamic numerical experiments aim at identifying the features of the redistribution of metals from scales close to that of their injection into the galactic halo scale of $\sim 10-20$ kpc. The first numerical models of this kind in which matter was injected by collective supernova bursts in the centers of galaxies were described in [230, 231, 234, 287, 296–300]. The resolution used in these models was still insufficient to describe physical processes on 'microscopic' scales close to the scale of injection of energy and mass by supernovae and the scale of thermal instability of the gas compressed by them, ~ 1 pc. In recent years, numerical models with such resolution have revealed some features of flows that are lost in phenomenological models with subgrid prescriptions.

In massive galaxies, not every breakthrough can trigger a significant outflow of mass from the galaxy. The problem is that even a slight asynchrony of supernova bursts, their spatial separation, or small perturbations lead to deformation of the shell surface, the rapid development of Rayleigh–Taylor instability and thermal instability due to radiation losses, and the formation of dense fragments of cooled gas and its settling under the influence of gravity onto the plane. These dynamic features are exhibited even in models with synchronized central SF bursts [226, 301]. This results in significant variations in the mass loading coefficient and its decrease for a given rate $\dot{M}_*$. The situation becomes more complicated if the regime of supernova bursts is more similar to the realistic stochastic one. One of the models of such a regime is a set of individual supernova bursts with total power L in volume $V_{\rm sf}$,

$$\frac{L}{V_{\rm sf}} = E_B \sum_i \delta(\mathbf{r} - \mathbf{r}_i, t - t_i)\,, \tag{5}$$

where the same energy $E_B = 10^{51}$ erg was assumed for all supernovae; supernovae were scattered randomly over a given SF volume $V_{\rm sf}$, and the moments of their bursts were distributed in time, depending on the mass of the pre-supernova. The lifetime of the pre-supernova $\tau_{\rm psn} = \tau_{\rm psn}(M_*)$ was set as a function of its mass, and the mass was randomly chosen so that the mass distribution of stars corresponded to the Salpeter function $\phi(m) \propto m^{-2.35}$ [132, 302, 303]. Figure 13 displays an example of suchlike outflow for various values of the spatial density of supernova explosions in a limited region of the galactic disk. It is easy to see that the outflow begins when the spatial density of supernovae exceeds a certain value ($1.4 \times 10^{-3}\, M_\odot$ per year), but, due to radiation losses, the flow breaks up into phases, and the densest and coldest of them settles downward, as can be seen from the velocity field.

The general pattern of outflow, divided into three phases, hot ($T > 10^5$ K), warm ($10^3 \leqslant T \leqslant 10^5$ K), and cold ($T < 10^3$ K), is illustrated in Fig. 14, which displays the mass-averaged time dependences of the flow rate of various gas phases. For large $\dot{M}_*$, the hot phase of insignificant mass ($T > 10^5$ K) flows out of the calculation zone and farther at a speed exceeding the escape velocity at times $t \geqslant 30$ Myr. The mass-dominant warm phase $10^3 < T \leqslant 10^5$ K, even at high SF rates, exhibits a loss of velocity at $t \gtrsim 10$ Myr; the cold phase with half the mass demonstrates quasi-periodic motion with a period of ~ 25 Myr. This corresponds to the cooled gas falling onto the plane being mixed with the gas remaining near the symmetry plane and then being pushed out again by shock waves.

It is of importance here that the part of the gas with the predominant mass, excluding the hot phase, has a vertical velocity of $v \lesssim 70$ km s^{-1} and therefore remains within the galaxy. Similar simulations at larger spatial scales, but with a lower numerical resolution, show that the vertical flow of the warm gas mass, driven by energy pumped from supernova bursts in the disk, falls very quickly with height, $\rho v \sim (1 + 2z/z_0)^{-4}$, where z_0 is the gas height scale. The hot-gas flow beyond one height scale remains constant until at least $z \gtrsim 10 z_0$ [304]. In general, numerical models of the dynamics of the outflow of enriched gas outside galaxies at the 'micro-level' show that the 'mass loading' of the outflows, i.e., the

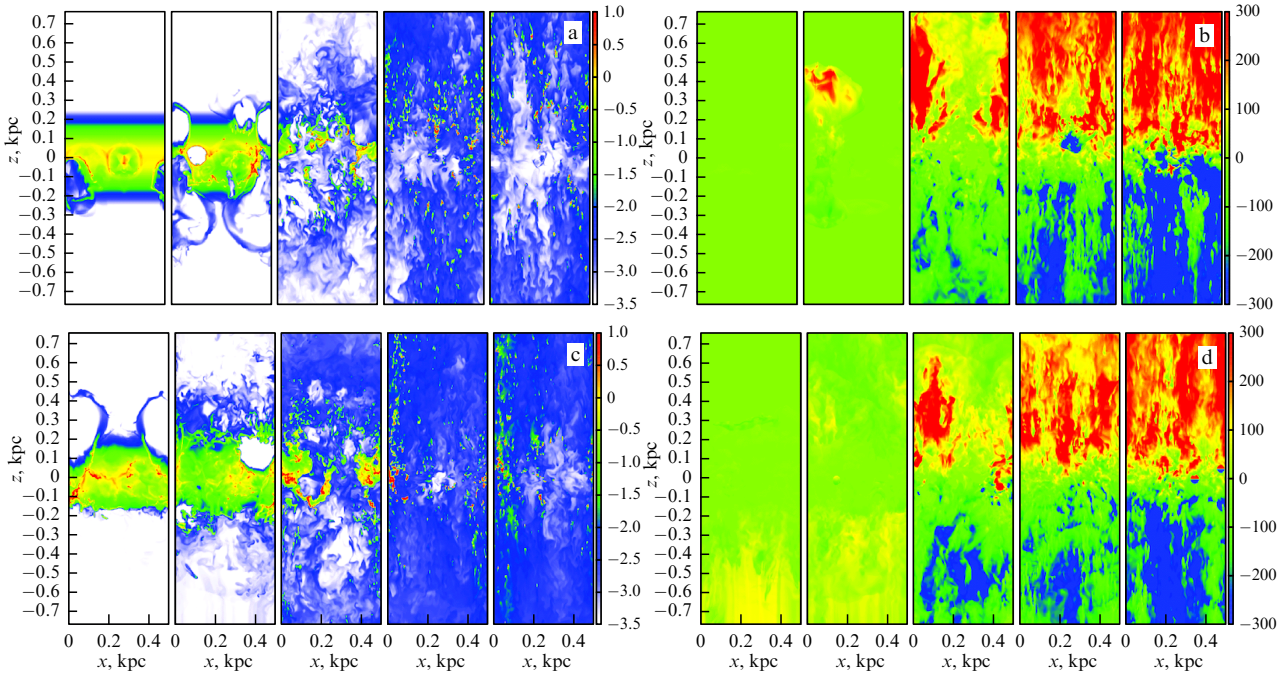

Figure 13. Vertical slice of the map of density (a, c) and velocity (b, d) for a flow induced by stochastic energy release from point sources (supernova bursts) randomly distributed in a volume with a base of 0.5×0.5 kpc and a vertical exponential scale of 0.1 kpc. Panels from left to right correspond to an SF rate of 1.4×10^{-4}, 4.2×10^{-4}, 1.4×10^{-3}, 4.2×10^{-3}, and $1.4 \times 10^{-2}\ M_\odot$ per year per base area. If recalculated for our Galaxy, this would correspond to values of $0.1, \ldots, 10\ M_\odot$ per year. (a, b) Dynamic state at time $t = 10$ Myr, (c, d) $t = 30$ Myr. (Figure taken from [132].)

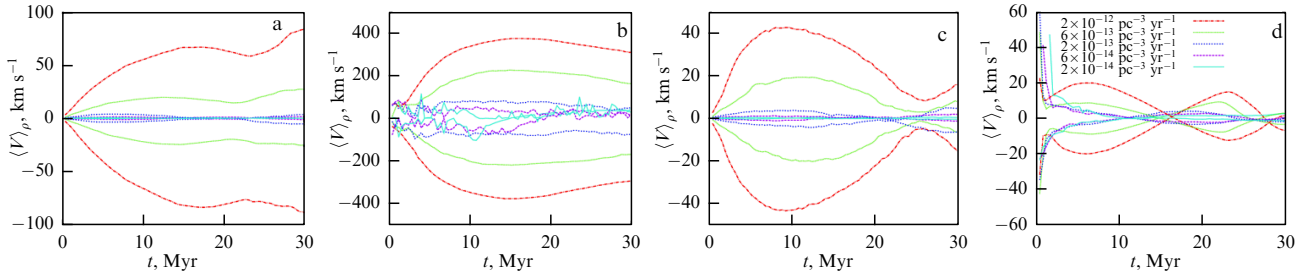

Figure 14. Time dependence of mass-averaged outflow velocities separated by phase: (a) gas in the entire temperature range, (b) hot-phase gas $T > 10^5$ K, (c) 'warm' gas $10^3 < T < 10^5$ K, and (d) cold phase $T \leqslant 10^3$ K. Number density of particles in the gas disk plane is $n_0 = 1$ cm^{-3}, palette in the upper-right corner of panel (d) corresponding to different SF rates is shown. (Figure taken from [132].)

ratio of the mass loss rate $\dot{M}$ to the star formation rate $\dot{M}_*$, is significantly lower than the measured values: it is $\eta \sim 0.1$ compared to estimated $\eta \sim 1-10$ provided by observations [220–222].

These two examples illustrate the problem of 'entraining' cold gas into motion or 'mass entrainment' in generally accepted terminology: acceleration of cold gas by a rarefied flow occurs $\sqrt{\chi}$ times more slowly than its disintegration $t_{ac}/t_{cc} \simeq \sqrt{\chi}$, where $t_{ac} \sim \chi R_c/v_c$ is the cloud acceleration time, $t_{cc} \sim \sqrt{\chi} R_c/v_c$ is the time of its disintegration, R_c is the radius of the cloud, v_c is its velocity relative to the rarefied gas flow, and $\chi = \rho_c/\rho_i$ is the ratio of the densities of the cold phase and the accelerating flow [305]. High-resolution numerical models [306–310] reveal the influence of nonlinear effects associated with the characteristics of the flow that emerges in the boundary layer between the cloud and the surrounding gas. This leads to the dependence of the time of mass loss of a cold cloud on the Mach number of the flow $t_{ac}/t_{cc} \propto \sqrt{1 + M_h}$ in models with radiation losses [307] and to the rapid fragmentation of multiphase cold condensates at the flow base [308]. As a result, fragments enriched in metals do not extend far beyond the enrichment domain. On the other hand, very rapid cooling of gas $t_{cool}/t_{cc} \ll 1$ can lead to an increase in the cold phase mass due to the condensation of the flowing gas on fragments enriched in metals. As a result, the exchange of momenta between the fragments and the flow moving around them becomes more intense, and the time during which such condensates are accelerated increases [306, 310, 311].

7. Mixing of metals

7.1 What is meant by mixing: illusory mixing

The chemical composition of a substance determines its equation of state, physical properties, and emissivity. Therefore, the mixing of matter, which provides the distribution of chemical elements over the volume of the region under consideration, is of fundamental importance for the entirety of astrophysics.

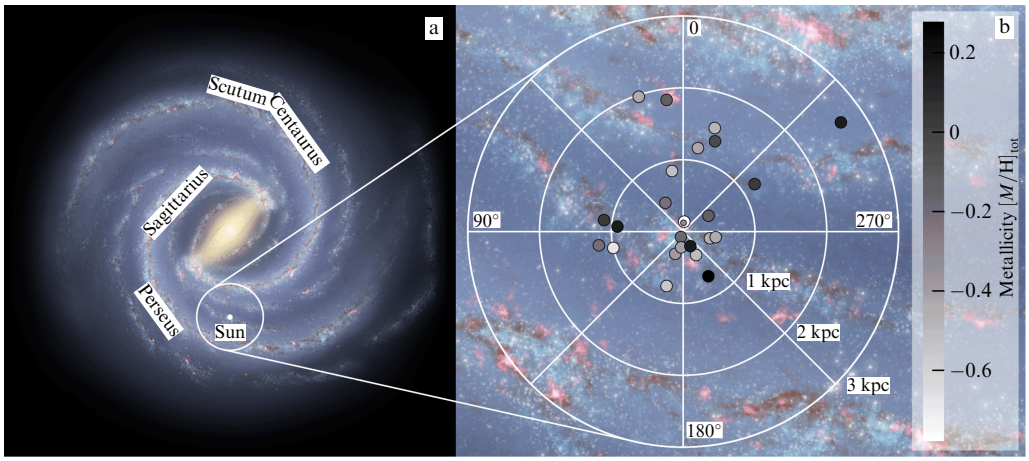

Figure 15. (a) Position of the Sun and the ISM in its vicinity with a radius of 3 kpc. (b) Enlarged view of this area, where dots show regions in which gas metallicities were measured. Color of the dots indicates the metallicity value on a logarithmic scale in accordance with the palette ruler on the right. (Figure taken from [315].)

The region of the Galaxy closest to us clearly shows a lack of mixing. This is indicated, for example, by the existence in a relatively close neighborhood of the Sun of a region with a characteristic size of ~ 3 kpc, where the content of iron in the various Cepheid stars[23] belonging to the population of a thin disk with ages ranging from 1 to 8 Gyr differs significantly, at least by half an order of magnitude. Since in this interval of ages the average abundance of metals in the Galaxy changed insignificantly (see Fig. 1), this may indicate a large time of mixing (several billion years) in the gas from which they arose [312, 313]. Variations in the elemental composition of this order are also exhibited by stars in various clusters and groups in our Galaxy (see, for example, [314]). Even greater differences in metallicity, one and a half orders of magnitude, were discovered recently in the interstellar medium in the vicinity of the Sun with a radius of 3 kpc [315]. It is of importance to note that variations in Z of half an order of magnitude or more occur, as can be seen in Fig. 15, on scales of only ~ 10 pc. This result is of fundamental importance for understanding that the physical properties and observational manifestations of cosmic plasma, including the properties of emerging stars, are determined by the *unmixed* chemical composition.

The term mixing is usually applied to more than one of various phenomena: the first implies fragmentary transfer ('splashing') of a chemical substance from a source over a large volume; the second refers to a nonuniform (irregular) flow of two immiscible liquids, which, if measured with insufficient resolution, can be perceived as a mixture; and the third is diffusion, homogenization of the mixture at the molecular level. The authors [138] were the first to pay attention to the terminological aspects of the concept of mixing in astrophysics. If chemical composition is measured with insufficient spatial resolution, terminological differences are insignificant. However, since the chemical composition determines the equation of state and emission and other characteristics, insufficient information about the degree of chemical heterogeneity can lead to an inadequate interpretation of observational data. An example of this situation could be a region of a gaseous medium within the angular resolution of a telescope, in which two regions are adjacent: one with a primordial chemical composition $Z = 0$, and the other enriched (in metals) $Z = Z_{\odot}$. Within the limits of angular resolution, the measured metallicity for the same emissivity of the regions will be $Z_{\rm obs} = \mu Z_{\odot}$, where μ is the mass fraction of the enriched region. In thermodynamic terms, the enriched part of the gas is fundamentally different from the gas with $Z = 0$, since it can radiatively cool to temperatures $T \sim 10$ K, while the region with the primordial gas can radiatively cool at best to $T \gtrsim 300$ K. Illusory mixing is especially important when the chemical composition of gas is measured in absorption lines: in this case, the chemical composition is determined by the sum of components through which the line of sight passes. Distinguishing of contributions is possible with additional independent observables, such as relative motions, line widths, and distinguishable ionization states, are available.

Possible, and in some cases unavoidable, effects of the lack of mixing are important for a correct understanding of evolutionary phenomena. An example is the differences in the chemical evolution of the IGM and galaxies in the same epochs. Figure 1 shows the apparent lag in the evolution of the IGM and galaxies in the distant ($z > 0.1$) Universe behind the Galaxy's populations. However, a correct interpretation of such a difference involves some caveats. It should be taken into account that enriched matter ejected from galaxies is always concentrated in fairly dense cloudlets and therefore mixes with the environment slowly. In observing the IGM in absorption lines, some of these cloudlets are lost due to their small geometric cross section. This guess is confirmed by direct observations of the distribution of metals in the IGM [294]. Therefore, the relative mass concentration of metals averaged over the entire IGM, which is discussed above, should be considered as a lower estimate of the metallicity of matter outside galaxies. This conclusion is also supported by direct observations of the distribution of the metallicity gradient along the filaments and caustics of a large-scale structure [316].

7.2 Mixing in the interstellar medium

Molecular diffusion in the ISM is ineffective when metals are mixed on scales comparable to or exceeding galactic scales. In the simplest case of an atomic medium with

[23] Cepheids are δ Cephei pulsating stars with a stable period–luminosity relationship.

temperature $T \sim 10^4$ K and diffusion coefficient $D \sim 10^{19} A^{-1/2} T_4^{1/2} n^{-1}$ cm^2 s^{-1}, where n is the gas density, A is the atomic number of the diffusing element, and $T_4 = T/(10^4\ \mathrm{K})$, the characteristic time for levelling chemical heterogeneity is $\tau_D \sim 10^{18} A^{1/2} R_l^2 T_4^{-1/2} n$ s, where the radius of the region of chemical inhomogeneity R_l is measured in parsecs. At densities $n \gtrsim 0.1$ cm^{-3} and scales $R_l \sim 1$ typical of the interstellar medium, the diffusion time is $\tau_D \gtrsim 10^{17}$ s, which is comparable to cosmological time. In a fully ionized medium with predominantly Coulomb collisions $D \sim 2.5 \times 10^{18} A^{-1/2} T_4^{5/2} n^{-1}$ cm^2 s^{-1}, the diffusion time is $\tau_D \sim 4 \times 10^{24} R_l^2 A^{1/2} T_4^{-5/2} n$ s, which, for gas scales in the halo and above $R_l \gtrsim 10^4$ and $T_4 \sim 10^2$, yields $\tau_D \gtrsim 4 \times 10^{21} R_l^2 n$ s. Therefore, starting from [317], 'turbulent' diffusion with a characteristic time of $\tau_t \sim L/v_t \sim 10$ Myr is discussed with $L \sim 100$ pc accepted as the characteristic size of a turbulent cell, $v_t \sim 10$ km s^{-1}, as the characteristic speed of chaotic movements in the ISM, and $D \sim L v_t$, as the diffusion coefficient. The first numerical model showed that the characteristic time of mixing of two passive scalar fields in the ISM under the effect of random shock waves from supernova explosions exceeds the above time by one and a half orders, $\tau \sim 300$ Myr [87].

It is worth stressing that steady state turbulence is commonly assumed under treating turbulent mixing. Actually, as was noted for the first time in [85, 86], turbulence in problems of mixing metals in galaxies and in the intergalactic medium is essentially *non steady state*. Indeed, the transfer of metals from a 'point' source to large scales begins with the ejection of an enriched cloud into the surrounding gas, where the cloud, under the influence of the Rayleigh–Taylor (RT) and Kelvin–Helmholtz (KH) instabilities, is getting destroyed and ejects some metals into the surrounding gas. Characteristic times of instabilities are $\tau_{RT} \sim \chi^{1/2} a/v$ and $\tau_{KH} \sim \chi a/v$ for Rayleigh–Taylor and Kelvin–Helmholtz, respectively, where, $\chi = \rho_c/\rho_i$ is the contrast of density in the cloud relative to the surrounding gas density, a is the radius of the cloud, and v is its speed.[24] The deceleration time of the cloud $\tau_{ac} \sim \chi a/v$ coincides in order of magnitude with the time τ_{KH} and exceeds the time τ_{RT} by a factor of $\chi^{1/2}$. In other words, the source of turbulence around the cloud — the energy of the relative motion of the cloud — is depleted at a characteristic time close to the time of the development of turbulence. The result is 'freeze-out' of mixing, when the development of instability ends at wavelengths for which molecular diffusion remains ineffective. This can be easily deduced from the transfer equation for chemical inhomogeneity, in our case, metallicity [318, 319]

$$\partial_t Z + \mathbf{u}(\mathbf{r}, t) \nabla Z = D \nabla^2 Z, \qquad (6)$$

where the right side describes the molecular diffusion of heavy elements. At the onset of the process, when molecular diffusion operates only at the cloud boundary, Eqn (6) is reduced to the equation of incompressible fluid $Z(\mathbf{r}, t) = \text{const}$ along the Lagrange trajectory. Mixing at the molecular level only begins when scales $\lambda < \sqrt{\chi a D/u}$ emerge in the perturbation spectrum; for the parameters of the circumgalactic shell adopted in [85, 86], this scale is $\lambda < 0.5 T_4^{1/2} n^{-1/2}$ pc, which is three orders of magnitude less than the thickness of the layer.

[24] Here, in estimating the time of Rayleigh–Taylor instability, the acceleration of the fragment associated with its slowdown is taken equal to $g \sim \chi^{-1} u^2/a$.

A more general analysis of the non steady state effects was carried out later in [320], where it was confirmed that the characteristic mixing time is greater than the dynamic time of the problem $\tau_{dyn} \sim L/v_{rms}$, where L is the scale of energy injection and v_{rms} is the mean square flow velocity. In the ISM of our Galaxy and similar galaxies, this condition is usually fulfilled: each element of the ISM gas is subjected to the action of a strong SW with a frequency $\nu_s(v) \sim 0.5 \times 10^{-4} \nu_{sn} v^{-1}$ [yr^{-1}], where v is the SW speed in [km s^{-1}] and ν_{sn} [yr^{-1}] is the frequency of supernova bursts in the galaxy [321]. For our Galaxy, this yields about $\nu_s^{-1}(v) \sim 0.5v$ Myr, which provides turbulence at a level sufficient for relatively rapid mixing on a scale of $\tau \sim 300$ Myr [87].

7.3 Mixing in the intergalactic medium

As noted above, the main mechanism of mixing of heavy elements in the intergalactic medium is associated with the Rayleigh–Taylor and Kelvin–Helmholtz instabilities. In the IGM, shear flows are the main type of flow that drives mixing. Multiple shock waves, similar to those that support mixing in ISM galaxies, are absent in the IGM, which results in a qualitatively different nature of mixing in these media. In particular, in the IGM, the mixing process is most effective only at initial times $t \sim \chi a/v$, while at intermediate times $\chi a/v < t \lesssim 10 \chi a/v$ the nature of the distribution of the chemical composition shows signs of 'freeze-out' in the above sense (see Section 7.2). Residual inhomogeneity in the spatial distribution of metals is not completely smoothed out over cosmological times, so a significant part of the metals remains confined in regions of relatively small sizes. The situation is even more aggravated if we take into account the radiation losses of the gas associated with the excitation of energy levels of heavy-element ions. The radiation loss rate is proportional to the relative concentration of heavy elements and the square of the gas density, $L(\rho, T, Z) \propto Z\rho^2$. This implies that the most metal-enriched regions lose thermal energy faster than those with low metal abundance. In the process of cooling, the gas is compressed by thermal and/or dynamic pressure of the surrounding gas, which, in turn, due to the ρ^2 factor, leads to even faster cooling and compression. As a result, fairly dense (and cold) compact gas condensates are formed. The probability of detecting such condensates should be extremely low due to the smallness of their geometric cross section.

7.4 Mixing in stripping off galaxy shells

In [85], a hydrodynamic description was developed for the spatial redistribution of metals when stripping off enriched galactic shells by the dynamic pressure of intergalactic gas. This process is clearly observed in galaxy clusters, where the stripping of galactic gas halos by dynamic pressure plays a significant role not only in the enrichment of the gas of clusters with metals but also in cluster ecosystems in general [322, 323]. As already noted, such shells are formed by explosive processes inside galaxies at the stages of star formation surges in their central regions [119–121]. When external intergalactic gas flows around a galaxy, the shell is carried away by the flow, deformed, and destroyed under the influence of instabilities caused by the relative motion of the shell gas and intergalactic gas: these are the Rayleigh–Taylor and Kelvin–Helmholtz instabilities.

A characteristic feature of the spatial distribution of metals that occurs in stripping off enriched shells is a high

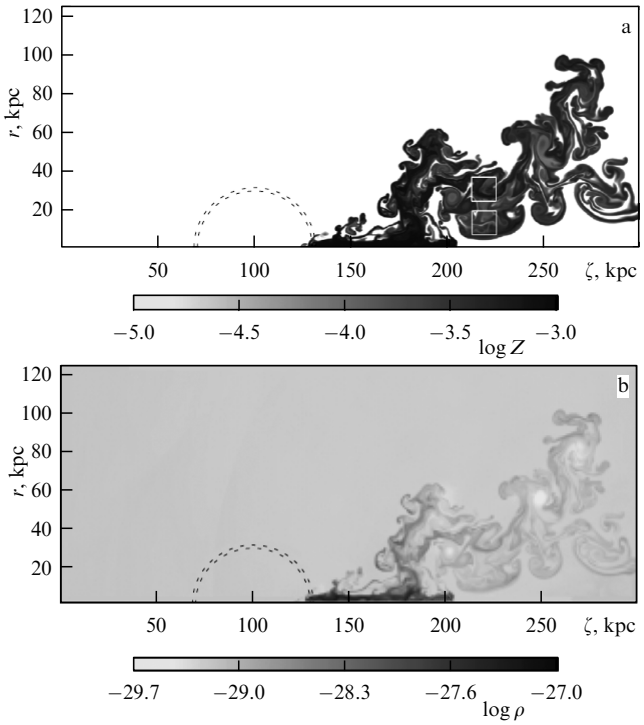

Figure 16. (a) Spatial distribution of metallicity in a flow around the outer enriched region of the galaxy; (b) gas density distribution in a flow at time $t \sim \chi^{1/2} a/v$ [85]. It can be easily seen that, although the shell has noticeably dissolved in the surrounding gas, i.e., the density in its individual fragments has practically equalized off the surrounding gas, the metallicity in the same fragments remains at a level close to the initial one.

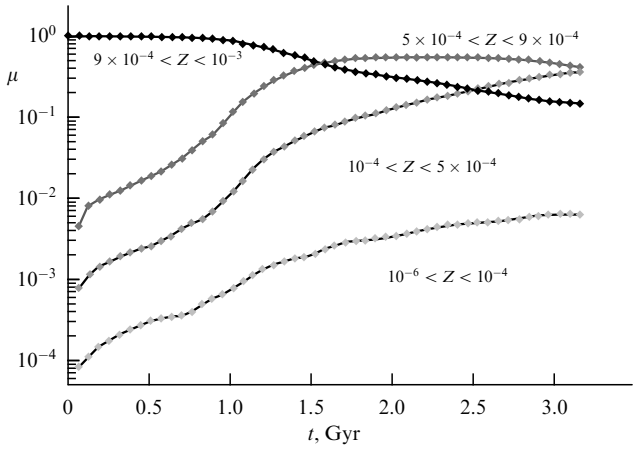

Figure 17. Fraction of the mass of metals contained in regions in a given range of metallicity; initial metallicity of the shell was taken equal to $Z = 10^{-3} Z_{\odot}$, $\tau_{ac} \sim 1$ Gyr, $\chi = 100$ [85].

degree of inhomogeneity that persists for long periods of time [85]. This is due to the above-mentioned 'freeze-out' effect of instabilities. When the shell is exposed to a flow of intergalactic gas, the development of instabilities leads to the separation and tearing away of fragments; further, they can be disintegrated into smaller fragments by the intergalactic gas flowing around. The mixing process can be presented as a hierarchical scheme of fragmentation of the shell under the effect of RT and KH instabilities. The fragmentation cascade continues while the relative velocity of the forming clouds and the intergalactic gas (IGG) flowing around them remains sufficiently large. However, such sequential fragmentation is accompanied by acceleration and entrainment of the cloud ensemble into the flow surrounding it, as a result of which the relative velocity of the shell gas and IGM decreases, and the fragmentation chain fades.[25]

At the ith stage of fragmentation, the relationships between the characteristic times of acceleration of the ith fragment by the incoming flow $\tau_{ac,i} \sim \chi a_i/u$ and the times of development of instabilities remain in the same proportion: $\tau_{ac,i} \sim \tau_{KH,i} \sim \chi^{1/2} \tau_{RT,i}$, since the most destructive effect is due to long-wave perturbations with a wavelength on the order of the fragment size [305]. Thus, the main contribution to cloud fragmentation is made by the Rayleigh–Taylor instability, but the number of successive fragmentations is limited by $\sqrt{\chi}$. After time τ_{ac} has elapsed, the set of fragments formed in such a cascade is carried away by the incoming flow of IGM gas, and the process stops. If we take into account that the interaction of the shell with the incoming flow at short times $t \sim \tau_{RT}$ leads to short-wave deformations of the cloud surface, the destructive effect of both instabilities increases due to the fact that the ratios of times τ_{RT} and τ_{KH} to τ_{ac} decrease as $\sim a_i/a$. Given this circumstance, the number of fragmentations and mixing efficiency increase, but remain limited [324]. An example of such 'frozen' fragmentation is shown in Fig. 16.

In the hierarchical fragmentation scheme presented above, each newly formed fragment is considered to be isolated, with which the unperturbed external flow continues to interact (a detailed description of such a scheme is given in [305]). In fact, after a certain event of shell fragmentation, the fragments interact not only with the external flow, which is also already disturbed, but also with each other, in particular, 'shading' each other and thereby reducing the shear flow velocity. An additional effect influencing the mixing process is the deformation of the surface of the fragments, which in turn leads to an increase in short-wave perturbations, further deforming the fragment surface. The consequence of this phenomenon is a significant increase in its surface and the force, which entrains the fragment along with the flow and reduces the relative velocity of the flow and the fragment. As a result, some fragments remain intact and, due to a decrease in the relative shear velocity, are actually inaccessible for subsequent mixing: 'bags' are formed with an almost unchanged or slowly changing metallicity.

As a result, a significant part of the shell metal mass remains concentrated in weakly mixed fragments, as shown in Fig. 17. It can be easily seen that, up to the moment $t \simeq \tau_{ac} \sim 1$ Gyr, fragments with the highest metallicity remain dominant in the mass of metals: $9 \times 10^{-4} < Z < 10^{-3}$. It is only at $t > \tau_{ac}$ that the main fraction of the mass of enriched regions is due to fragments with $5 \times 10^{-4} < Z < 9 \times 10^{-4}$. The volume-dominant metal-poor regions $Z < 5 \times 10^{-4}$ contain a mass of less than 30%. Figure 18 shows the dependence of the volume occupied by regions with a given metallicity $V(Z)$ for two different times.

[25] In [85], a model of a shell with a radius of 30 kpc and a thickness of 1 kpc was examined. When more extended regions of the circumgalactic halo are stripped off, quantitative differences may appear that are associated with the later manifestation of the effects of molecular (or numerical) diffusion on small scales. However, the conclusion about depressed mixing as a result of the 'freeze-out' of instabilities persists.

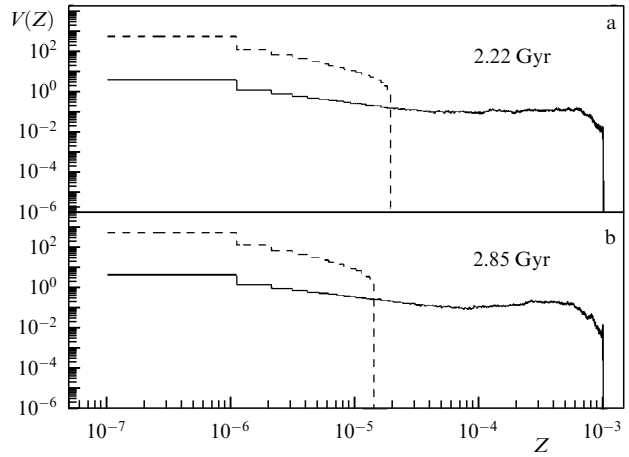

Figure 18. Distribution of $Z(t)$ over the volume; solid line corresponds to the results of direct modeling, while dashed line shows the distribution of metallicity should it be described by turbulent diffusion with coefficient $\kappa = \langle u \rangle R_s/3 \sim 10^{29}$ cm^2 s^{-1}, corresponding to parameters of the turbulent flow established in the flow moving around at $t = 2.22$ (a) and $t = 2.85$ (b) Gyr. (Figures taken from [85].)

The dashed lines show the metallicity distribution functions in the case where the mixing was diffusive with the diffusion coefficient determined by the turbulence parameters in the region of interaction of the IGM with the shell around the galaxy $D_t \sim \langle \Delta a_s \rangle \langle u \rangle$, where $\langle \Delta a_s \rangle$ is the characteristic thickness of the turbulent shell. Unlike the turbulent diffusion model, where the maximum value of metallicity in a region decreases as $\propto t^{-1/2}$, in the dynamic model, the maximum metallicity, which is close to the initial value, remains in enriched regions almost unchanged, $\Delta V(Z \geqslant 6 \times 10^{-4})/V(Z) \sim 0.1$.

An illustration of ineffective mixing in the dynamic model is a significant excess (by two orders of magnitude) of the volume of regions with low metallicity $Z < 5 \times 10^{-4}$ over the volume of regions with high metallicity $Z \geqslant 9 \times 10^{-4}$. As noted in Section 4.2, in this case, the probability that a high-metallicity region crosses the line of sight decreases as $P \propto Z^{-2/\alpha}$, where $\alpha \simeq 2/3$ is the power exponent of the decrease in metallicity with radius. This result, obtained for the first time in numerical modeling [85, 86], was subsequently confirmed in observations [191]. In calculating metals in the Universe using absorption spectra, the $P \propto Z^{-2/\alpha}$ effect can lead to their significant underestimation. This circumstance is directly related to the problem of 'hidden metals' discussed above (see Section 4.2).

Another distinctive feature of ineffective mixing in dynamic models, which is confirmed by observations, is the extremely weak dependence of metallicity on density. As can be seen in Fig. 16, the cloud of enriched gas at short times $t < \chi^{-1/2}\tau_{ac}$ expands and propagates over increasingly larger volumes, but is not mixed, due to the characteristic sizes of the fragments remaining significantly larger than the diffusion ones. As the cloud expands, its density becomes comparable to that of the surrounding IGG (intergalactic gas), but the cloud remains identifiable by its high metallicity.[26] The resulting dependence $Z(\rho)$ turns out to be flat, as shown in Fig. 19.

[26] The sharp decrease in metallicity at the lower density limit is related to numerical diffusion.

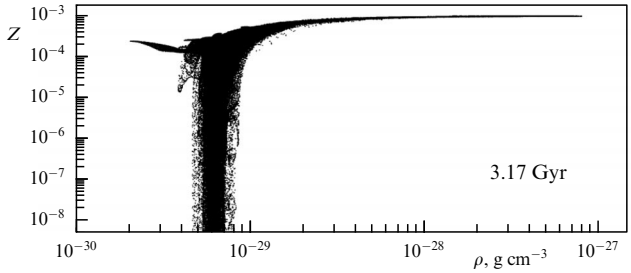

Figure 19. Metallicity Z as a function of enriched gas density ρ. (Figure taken from [85].)

It should be emphasized that, in contrast to the ISM, where each gas element is subjected to the action of an SW from supernovae fairly frequently, $\Psi(> v) \sim 2 \times 10^{-8} v_{100}^{-1}$ yr^{-1}, $v_{100} = v/100$ km s^{-1} [321], in the IGM, the density of strong SWs is small [325]. With each such event, the enriched gas is enveloped by a flow moving at a speed significantly different from that of the gas element itself, and thus the conditions for the development of RT and KH instabilities are renewed each time. In the IGM, the frequency of arrival of strong shock waves is significantly lower; therefore, each element of the IGM, including enriched fragments, can be subject to the strong influence of a shear or accelerating flow, at best, once, due to which the RT and KN instabilities are frozen-out. Typical velocities of turbulent motions in the IGM, expected from a strong galactic wind, are only $\sim 1-2$ km s^{-1} [325], which is unlikely to make a significant contribution to mixing.

8. Conclusions and prospects

8.1 Discussion and conclusions

Enrichment. The heavy elements observed in the intergalactic medium at redshifts ranging from $z \simeq 1.5$ to $z \simeq 6$ are the result of the activity of stars (supernova bursts) in the very early ($z \gtrsim 9$) Universe and the subsequent redistribution of nucleosynthesis products throughout the Universe, starting from $z \lesssim 6$. The efficiency of the initial stages of stellar nucleosynthesis was so high that the amount of metal produced in the early Universe may have exceeded the actually observed value. The high degree of inhomogeneity in the distribution of metals in early galaxies and in the intergalactic medium and the uncertain ionization evolutionary state of the gas may be directly related to the fact that some metals are hidden in forms that are not yet observable.

Mixing. The action of gas-dynamic mechanisms of the transfer of heavy elements into the intergalactic medium and their subsequent mixing, apparently, is limited in a natural way by the scales on which the Rayleigh–Taylor and Kelvin–Helmholtz instabilities responsible for mixing are frozen-out. These scales are usually only several times larger than the original scale of the enriched region, due to which the distribution of metals in the IGM remains extremely inhomogeneous, which is in fact observed. This distribution pattern also persists if heavy elements are ejected from galaxies in the form of dust particles by the stellar radiation pressure, especially if we take into account that charged dust particles can be retained by the magnetic field of galaxies and the circumgalactic medium. Extended circumgalactic halos ($\sim 100-200$ kpc) are essentially a transition region between galaxies and the intergalactic medium, but what specific

mechanisms are responsible for the transfer of metals within this region is still not clear.

'*Diffuse*' *intergalactic medium*. The amount of heavy elements in the diffusive intergalactic medium, i.e., in the environment outside galaxy clusters, is only $Z \sim 10^{-2} Z_{\odot}$, judging by those regions that contribute to absorption in the Lyα forest. It is possible that a significant part of heavy elements is contained in small-scale condensates with an increased concentration of heavy elements, as follows from numerical experiments [85, 86] and observations [191]. A possible indication favoring this option may be the recently discovered sharp increase in the amount of CIV at $z < 2.5$ [151, 154, 326], possibly associated with the expansion (or evaporation) of small-sized clouds with increased metallicity.

Clusters of galaxies. The high metallicity of the gas of clusters and, apparently, groups of galaxies (with $Z \sim 0.3 Z_{\odot}$) indicates that such systems chemically evolved in a way fundamentally different from that of the matter outside the clusters. These differences are essentially determined by the features of gas dynamics in the clusters: (a) more efficient close tidal interactions between galaxies, stimulating the loss of gas and star formation in them and, consequently, more effective mixing of enriched gas; (b) the enhanced stripping of the outer gas halos of galaxies by the dynamic pressure of the surrounding gas, and (c) finally, the fact that the gas in galaxy clusters is significantly hotter than that outside the clusters. The last circumstance may be of importance for the evaporation of small-scale over-enriched gas condensates ejected by galaxies and, as a result, for their more efficient mixing (see discussion in [323]). The absence of correlations between the metallicity of gas in clusters and their dynamic characteristics apparently indicates that the enrichment process in clusters has been completed.

8.2 Prospects for new observations

As already noted, in solving the problems discussed, the role of observational instruments in the widest range of the electromagnetic spectrum from the X-ray (see, for example, [327]) to the (sub)millimeter range [328] is of critical importance.

The ultraviolet, submillimeter, and infrared ranges of the spectrum provide the richest information about the chemical composition of matter: the overwhelming majority of the results described above have been obtained by exploring these parts of the spectrum. The recently launched James Webb Space Telescope[27] is already yielding results: galaxies have been detected in the range $z = 10-16$ with metallicity $Z \sim (0.01-0.1) Z_{\odot}$ and no traces of evolution throughout the entire period [128], apparently associated with the removal of dust from galaxies under the influence of short-term episodes of the galactic wind [329, 300]. In any case, the first JWST results suggest a scenario in which the transition of the Universe from 'dark ages,' when it was only ~ 250 Myr ($z \sim 16$), to the modern era is full of turbulent events associated with the formation of the first stars and the generation of the first portions of starlight and heavy chemical elements. We can therefore hope that the next decade will bring many revolutionary new ideas about the 'dawn' of the Universe.

Among the upcoming developments in this area, we focus on several projects planned for the near future. In Russia, the Spektr-UF space observatory is scheduled to be launched in the end of 2020s (see [331, 332]). The preliminary scientific program for the observatory includes observations that can make a significant contribution to solving some of the problems described in this review [333]. In what regards, for example, hidden metals, it is planned to:

- carry out observations with high spectral resolution of new and already known regions of warm-hot intergalactic gas and extended halos around galaxies;
- conduct a detailed study of the dependence of metallicity on the size and other physical characteristics of metal-containing regions, which will make it possible to correctly take into account the effects of observational selection due to a possible correlation between metallicity and size.

In the mid-2030s, it is planned to launch the *Millimetron* space observatory into orbit as part of the Spektr-M international project, which aims at studying the Universe in the range $\lambda = 50-1000$ μm, inaccessible for ground-based observations [334–336]. In what regards the enrichment of the Universe with metals, the *Millimetron* observatory will:

- examine early episodes of star formation in the activity of galactic nuclei in the epoch $z \simeq 7-10$ in the fine structure lines of heavy elements [337, 338];
- explore galaxies and their nuclei obscured by dust in the optical and near-IR ranges [339–341];
- study in detail the formation and circulation of dust in ultra-luminous IR galaxies by examining the 'laboratory' closest to us, the Arp 220 galaxy, located at a distance of 77 Mpc, which contains two active nuclei, with an optical thickness in the far IR range of $\tau_{0.5\,\mathrm{mm}} \gtrsim 1$.

[27] This part of the text was written on September 3, 2022.

Acknowledgments

Various issues presented in this review were discussed at different times with S A Balashev, N G Bochkarev, R-J Dettmar, A Ferrara, B B Nath, P Noterdaeme, and Peng Oh. We are very grateful to them for their interest, friendly criticism, and advice. We also thank the reviewers for their constructive comments. Work by Yu A Shchekinov was part of project 41-2020, New Research Groups of the Lebedev Physical Institute and the Program of the Presidium of the Russian Academy of Sciences (project code 28). Work by E O Vasiliev and B M Shustov was partially supported by the Russian Science Foundation (grant 19-72-20089).

References

1. Chandrasekhar S, Gamow G, Tuve M A *Nature* **141** 982 (1938)
2. Bethe H A *Phys. Rev.* **55** 434 (1939)
3. Gamow G *Phys. Rev.* **70** 572 (1946)
4. Salpeter E E *Annu. Rev. Nucl. Sci.* **2** 41 (1953)
5. Cyburt R H et al. *Rev. Mod. Phys.* **88** 015004 (2016)
6. Tayler R J *Rep. Prog. Phys.* **29** 489 (1966)
7. Trimble V *Rev. Mod. Phys.* **47** 877 (1975)
8. Rolfs C, Trautvetter H P, Rodney W S *Rep. Prog. Phys.* **50** 233 (1987)
9. Nomoto K, Kobayashi C, Tominaga N *Annu. Rev. Astron. Astrophys.* **51** 457 (2013)
10. Bertulani C A, Kajino T *Prog. Part. Nucl. Phys.* **89** 56 (2016)
11. Bensby T, Feltzing S, Oey M S *Astron. Astrophys.* **562** A71 (2014)
12. Feltzing S, Chiba M *New Astron. Rev.* **57** 80 (2013)
13. Rebassa-Mansergas A et al. *Mon. Not. R. Astron. Soc.* **505** 3165 (2021)
14. Mardini M K et al. *Astrophys. J.* **936** 78 (2022); arXiv:2206.08459
15. Aravena M et al. *Astrophys. J.* **833** 71 (2016)
16. Rojas-Ruiz S et al. *Astrophys. J.* **891** 146 (2020)

17. Roberts-Borsani G et al. *Astrophys. J.* **927** 236 (2022)
18. Tacchella S et al. *Astrophys. J.* **927** 170 (2022)
19. De Cia A et al. *Astron. Astrophys.* **611** A76 (2018)
20. Poudel S et al. *Mon. Not. R. Astron. Soc.* **473** 3559 (2018)
21. Fukugita M, Peebles P J E *Astrophys. J.* **616** 643 (2004)
22. Songaila A *Astrophys. J.* **561** L153 (2001)
23. Codoreanu A et al. *Mon. Not. R. Astron. Soc.* **481** 4940 (2018)
24. Tumlinson J et al. *Science* **334** 948 (2011)
25. Renzini A *Astrophys. J.* **488** 35 (1997)
26. Soderblom D R *Annu. Rev. Astron. Astrophys.* **48** 581 (2010)
27. Wyse R F G, Gilmore G *Astron. J.* **110** 2771 (1995)
28. Rosenberg A et al. *Astron. J.* **118** 2306 (1999)
29. Gratton R, Sneden C, Carretta E *Annu. Rev. Astron. Astrophys.* **42** 385 (2004)
30. Forbes D A et al. *Mon. Not. R. Astron. Soc.* **366** 1230 (2006)
31. Nozawa T et al., in *Low-Metallicity Star Formation: From the First Stars to Dwarf Galaxies* (Proc. of the Intern. Astron. Union, Vol. 4, Iss. S255, Eds L K Hunt, S C Madden, R Schneider) (Cambridge: Cambridge Univ. Press, 2008) p. 254; arXiv:0809.4369
32. Kabanov A A, Shustov B M *Astron. Rep.* **55** 784 (2011); *Astron. Zh.* **88** 852 (2011)
33. Wyse R F G et al. *Astrophys. J.* **639** L13 (2006)
34. Deason A J et al. *Astrophys. J.* **763** 113 (2013)
35. Belokurov V *New Astron. Rev.* **57** 100 (2013)
36. Beers T C, Christlieb N *Annu. Rev. Astron. Astrophys.* **43** 531 (2005)
37. Frebel A *Annu. Rev. Nucl. Part. Sci.* **68** 237 (2018)
38. Christlieb N et al. *Nature* **419** 904 (2002)
39. Matijevič G et al. *Astron. Astrophys.* **603** A19 (2017)
40. Tegmark M et al. *Astrophys. J.* **474** 1 (1997)
41. Abel T, Bryan G L, Norman M L *Science* **295** 93 (2001)
42. Bromm V, Coppi P S, Larson R B *Astrophys. J.* **564** 23 (2002)
43. Umeda H, Nomoto K *Nature* **422** 871 (2003)
44. Tan J C, McKee C F *Astrophys. J.* **603** 383 (2004)
45. Susa H, Hasegawa K, Tominaga N *Astrophys. J.* **792** 32 (2014)
46. Hirano S et al. *Mon. Not. R. Astron. Soc.* **448** 568 (2015)
47. Hirano S, Bromm V *Mon. Not. R. Astron. Soc.* **470** 898 (2017)
48. Murphy L J et al. *Mon. Not. R. Astron. Soc.* **501** 2745 (2021)
49. Bromm V et al. *Mon. Not. R. Astron. Soc.* **328** 969 (2001)
50. Bromm V, Loeb A *Nature* **425** 812 (2003)
51. Schneider R et al. *Nature* **422** 869 (2003)
52. Schneider R et al. *Mon. Not. R. Astron. Soc.* **369** 1437 (2006)
53. Vasiliev E O et al. *Astron. Rep.* **56** 895 (2012); *Astron. Zh.* **89** 987 (2012)
54. Tsujimoto T, Shigeyama T *Astrophys. J. Lett.* **795** L18 (2014)
55. Ritter J S et al. *Mon. Not. R. Astron. Soc.* **451** 1190 (2015)
56. Nagakura T, Omukai K *Mon. Not. R. Astron. Soc.* **364** 1378 (2005)
57. Vasil'ev E O, Shchekinov Yu A *Astron. Rep.* **49** 587 (2005); *Astron. Zh.* **82** 659 (2005)
58. Vasiliev E O, Shchekinov Yu A *Astrophysics* **48** 491 (2005); *Astrofizika* **48** 585 (2005)
59. Shchekinov Yu A, Vasiliev E O *Mon. Not. R. Astron. Soc.* **368** 454 (2006)
60. Glover S C O, Brand P W J L *Mon. Not. R. Astron. Soc.* **340** 210 (2003)
61. Shchekinov Yu A, Vasiliev E O *Astron. Astrophys.* **419** 19 (2004)
62. Vasiliev E O, Shchekinov Yu A *Astron. Rep.* **50** 778 (2006); *Astron. Zh.* **83** 872 (2006)
63. Yoshida N, Omukai K, Hernquist L *Science* **321** 669 (2008)
64. Hummel J A et al. *Mon. Not. R. Astron. Soc.* **453** 4136 (2015)
65. Hummel J A, Stacy A, Bromm V *Mon. Not. R. Astron. Soc.* **460** 2432 (2016)
66. Wollenberg K M J et al. *Mon. Not. R. Astron. Soc.* **494** 1871 (2020)
67. Tsujimoto T, Shigeyama T, Yoshii Y *Astrophys. J.* **519** L63 (1999)
68. Deal M, Richard O, Vauclair S *Astron. Astrophys.* **646** A160 (2021)
69. Arbey A, Auffinger J, Silk J *Phys. Rev. D* **102** 023503 (2020)
70. Sanderbeck P U, Bird S, Haiman Z *Phys. Rev. D* **104** 103022 (2021)
71. Tumlinson J *Astrophys. J.* **641** 1 (2006)
72. Simon J D, Geha M *Astrophys. J.* **670** 313 (2007)
73. Harris W E *Astron. J.* **112** 1487 (1996)
74. Ferrara A, Tolstoy E *Mon. Not. R. Astron. Soc.* **313** 291 (2000)
75. Bovill M S, Ricotti M *Astrophys. J.* **693** 1859 (2009)
76. Kirby E N et al. *Astrophys. J.* **727** 78 (2011)
77. Collins M L M, Read J I *Nat. Astron.* **6** 647 (2022)
78. Ricotti M *Mon. Not. R. Astron. Soc.* **392** L45 (2009)
79. Ji A et al. *Bull. Am. Astron. Soc.* **51** 166 (2019)
80. Heger A, Woosley S E *Astrophys. J.* **724** 341 (2010)
81. Skúladóttir Á et al. *Astrophys. J. Lett.* **915** L30 (2021)
82. Annibali F, Tosi M *Nat. Astron.* **6** 48 (2022)
83. Skúladóttir Á et al. *Astron. Astrophys.* **615** A137 (2018)
84. Quiret S et al. *Mon. Not. R. Astron. Soc.* **458** 4074 (2016)
85. Dedikov S Yu, Shchekinov Yu A *Astron. Rep.* **48** 9 (2004); *Astron. Zh.* **81** 11 (2004)
86. Vasiliev E O, Dedikov S Yu, Shchekinov Yu A *Astrophys. Bull.* **64** 317 (2009); *Astrofiz. Byull.* **64** 333 (2009)
87. de Avillez M A, Mac Low M M *Astrophys. J.* **581** 1047 (2002)
88. Becker R H et al. *Astron. J.* **122** 2850 (2001)
89. Djorgovski S G et al. *Astrophys. J.* **560** L5 (2001)
90. Fan X et al. *Astron. J.* **123** 1247 (2002)
91. Songaila A *Astron. J.* **127** 2598 (2004)
92. Bolton J S, Haehnelt M G *Mon. Not. R. Astron. Soc.* **429** 1695 (2013)
93. Planck Collab., Ade P A R et al. *Astron. Astrophys.* **594** A13 (2016)
94. Madau P, Haardt F, Rees M J *Astrophys. J.* **514** 648 (1999)
95. Loeb A, Barkana R *Annu. Rev. Astron. Astrophys.* **39** 19 (2001)
96. Ciardi B, Ferrara A *Space Sci. Rev.* **116** 625 (2005)
97. Gnedin N Y *Astrophys. J.* **535** 530 (2000)
98. Ciardi B, Madau P *Astrophys. J.* **596** 1 (2003)
99. Furlanetto S R, Oh S P *Mon. Not. R. Astron. Soc.* **363** 1031 (2005)
100. Zhu Y et al. *Astrophys. J.* **932** 76 (2022)
101. Fan X et al. *Astron. J.* **132** 117 (2006)
102. Fan X, Carilli C L, Keating B *Annu. Rev. Astron. Astrophys.* **44** 415 (2006)
103. Zaroubi S, in *The First Galaxies. Theoretical Predictions and Observational Clues* (Astrophysics and Space Science Library, Vol. 396, Eds T Wiklind, B Mobasher, V Bromm) (Berlin: Springer-Verlag, 2013) p. 45; arXiv:1206.0267
104. Barkana R *Phys. Rep.* **645** 1 (2016)
105. Robertson B E *Annu. Rev. Astron. Astrophys.* **60** 121 (2022); arXiv:2110.13160
106. Inoue A K et al. *Publ. Astron. Soc. Jpn.* **70** 55 (2018)
107. Harikane Y et al. *Astrophys. J.* **883** 142 (2019)
108. Becker G D, Rauch M, Sargent W L W *Astrophys. J.* **698** 1010 (2009)
109. Becker G D et al. *Astrophys. J.* **744** 91 (2012)
110. Oesch P A et al. *Astrophys. J.* **819** 129 (2016)
111. Jiang L et al. *Nat. Astron.* **5** 262 (2021)
112. Hamann F et al. *Astrophys. J.* **564** 592 (2002)
113. Sniegowska M et al. *Astrophys. J.* **910** 115 (2021)
114. Wang S et al. *Astrophys. J.* **925** 121 (2022)
115. Jiang L et al. *Astron. J.* **134** 1150 (2007)
116. De Rosa G et al. *Astrophys. J.* **790** 145 (2014)
117. Moiseev A V et al. *Astron. Rep.* **48** 367 (2004); *Astron. Zh.* **81** 403 (2004)
118. Nath B B, Trentham N *Mon. Not. R. Astron. Soc.* **291** 505 (1997)
119. Ferrara A, Pettini M, Shchekinov Yu *Mon. Not. R. Astron. Soc.* **319** 539 (2000)
120. Madau P, Ferrara A, Rees M J *Astrophys. J.* **555** 92 (2001)
121. Scannapieco E, Ferrara A, Madau P *Astrophys. J.* **574** 590 (2002)
122. Pinsonneault S, Martel H, Pieri M M *Astrophys. J.* **725** 2087 (2010)
123. Hashimoto T et al. *Nature* **557** 392 (2018)
124. Salvaterra R et al. *Nature* **461** 1258 (2009)

125. Harikane Y et al. *Astrophys. J.* **929** 1 (2022)
126. Harikane Y et al. *Astrophys. J. Suppl.* **265** 5 (2023); arXiv:2208.01612
127. Finkelstein S L et al. *Astrophys. J. Lett.* **940** L55 (2022); arXiv:2207.12474
128. Furtak L J et al. *Mon. Not. R. Astron. Soc.* **519** 3064 (2023); arXiv:2208.05473
129. Wu X B et al. *Nature* **518** 512 (2015)
130. Bañados E et al. *Nature* **553** 473 (2018)
131. Inayoshi K, Visbal E, Haiman Z *Annu. Rev. Astron. Astrophys.* **58** 27 (2020)
132. Vasiliev E O, Shchekinov Yu A, Nath B B *Mon. Not. R. Astron. Soc.* **486** 3685 (2019)
133. Kormendy J, Ho L C *Annu. Rev. Astron. Astrophys.* **51** 511 (2013)
134. Venemans B P et al. *Astrophys. J.* **845** 154 (2017)
135. Venemans B P et al. *Astrophys. J. Lett.* **874** L30 (2019)
136. Madau P *AIP Conf. Proc.* **393** 481 (1997); astro-ph/9612157
137. Madau P, Dickinson M *Annu. Rev. Astron. Astrophys.* **52** 415 (2014)
138. Dayal P, Ferrara A *Phys. Rep.* **780–782** 1 (2018)
139. Ciardi B et al. *Mon. Not. R. Astron. Soc.* **314** 611 (2000)
140. Miralda-Escudé J, Rees M J *Astrophys. J.* **478** L57 (1997)
141. Kashikawa N et al. *Astrophys. J.* **761** 85 (2012)
142. Dayal P et al. *Mon. Not. R. Astron. Soc.* **445** 2545 (2014)
143. Pettini M et al. *Astrophys. J.* **594** 695 (2003)
144. Simcoe R A et al. *Astrophys. J.* **743** 21 (2011)
145. D'Odorico V et al. *Mon. Not. R. Astron. Soc.* **435** 1198 (2013)
146. Boksenberg A, Sargent W L W *Astrophys. J. Suppl.* **218** 7 (2015)
147. Díaz C G et al. *Boletin Asoc. Argentina Astron. La Plata Argentina* **58** 54 (2016)
148. Shull J M, Danforth C W, Tilton E M *Astrophys. J.* **796** 49 (2014)
149. Cooksey K L et al. *Astrophys. J.* **729** 87 (2011)
150. Scannapieco E et al. *Mon. Not. R. Astron. Soc.* **365** 615 (2006)
151. D'Odorico V et al. *Mon. Not. R. Astron. Soc.* **512** 2389 (2022)
152. Pallottini A et al. *Mon. Not. R. Astron. Soc.* **440** 2498 (2014)
153. Ryan-Weber E V et al. *Mon. Not. R. Astron. Soc.* **395** 1476 (2009)
154. D'Odorico V et al. *Mon. Not. R. Astron. Soc.* **401** 2715 (2010)
155. Rauch M *Annu. Rev. Astron. Astrophys.* **36** 267 (1998)
156. Wolfe A M, Gawiser E, Prochaska J X *Annu. Rev. Astron. Astrophys.* **43** 861 (2005)
157. Krogager J K et al. *Mon. Not. R. Astron. Soc.* **469** 2959 (2017)
158. Rhodin N H P et al. *Mon. Not. R. Astron. Soc.* **506** 546 (2021)
159. Rahmati A, Schaye J *Mon. Not. R. Astron. Soc.* **438** 529 (2014)
160. De Cia A et al. *Astron. Astrophys.* **596** A97 (2016)
161. Rafelski M et al. *Astrophys. J.* **755** 89 (2012)
162. Somerville R S, Davé R *Annu. Rev. Astron. Astrophys.* **53** 51 (2015)
163. Naab T, Ostriker J P *Annu. Rev. Astron. Astrophys.* **55** 59 (2017)
164. Cen R, Ostriker J P *Astrophys. J.* **429** 4 (1994)
165. Petitjean P, Mueket J P, Kates R E *Astron. Astrophys.* **295** L9 (1995)
166. Zhang Y, Anninos P, Norman M L *Astrophys. J.* **453** L57 (1995)
167. Hernquist L et al. *Astrophys. J.* **457** L51 (1996)
168. Hui L, Gnedin N Y, Zhang Y *Astrophys. J.* **486** 599 (1997)
169. Bi H, Davidsen A F *Astrophys. J.* **479** 523 (1997)
170. Theuns T, Leonard A, Efstathiou G *Mon. Not. R. Astron. Soc.* **297** L49 (1998)
171. Davé R et al. *Astrophys. J.* **511** 521 (1999)
172. Shen J et al. *Astrophys. J.* **645** 783 (2006)
173. Libeskind N I et al. *Mon. Not. R. Astron. Soc.* **473** 1195 (2018)
174. Demiański M I, Doroshkevich A G, Larchenkova T I *Astron. Lett.* **46** 359 (2020)
175. Martizzi D et al. *Mon. Not. R. Astron. Soc.* **486** 3766 (2019)
176. Martizzi D et al. *Mon. Not. R. Astron. Soc.* **491** 5747 (2020)
177. Tytler D et al., in *QSO Absorption Lines. Proc. of the ESO Workshop, Garching, Germany, 21–24 November 1994* (ESO Astrophysics Symp., Vol. 289, Ed. G Meylan) (Berlin: Springer-Verlag, 1995) p. 289
178. Cowie L L et al. *Astron. J.* **109** 1522 (1995)
179. Becker G D "A high-resolution study of the high-redshift intergalactic medium", Ph.D. Thesis (Pasadena, CA: California Institute of Technology, 2007)
180. Juarez Y et al. *Astron. Astrophys.* **494** L25 (2009)
181. Savaglio S, in *Low-Metallicity Star Formation: From the First Stars to Dwarf Galaxies* (Proc. of the Intern. Astron. Union, Vol. 4, Iss. S255, Eds L K Hunt, S C Madden, R Schneider) (Cambridge: Cambridge Univ. Press, 2008) p. 204; arXiv:0808.2917
182. Schaye J et al. *Astrophys. J.* **541** L1 (2000)
183. Schaye J et al. *Astrophys. J.* **596** 768 (2003)
184. Ricotti M, Gnedin N Y, Shull J M *Astrophys. J.* **534** 41 (2000)
185. Hoyle F et al. *Astrophys. J.* **620** 618 (2005)
186. Kreckel K, Joung M R, Cen R *Astrophys. J.* **735** 132 (2011)
187. Pan D C et al. *Mon. Not. R. Astron. Soc.* **421** 926 (2012)
188. Ohyama Y et al. *Astrophys. J.* **591** L9 (2003)
189. Bischetti M et al. *Astron. Astrophys.* **630** A59 (2019)
190. Watson W E, Vogeley M S, arXiv:2204.06708
191. Schaye J, Carswell R F, Kim T S *Mon. Not. R. Astron. Soc.* **379** 1169 (2007)
192. Schaye J *Astrophys. J.* **559** 507 (2001)
193. Vasiliev E O *Mon. Not. R. Astron. Soc.* **414** 3145 (2011)
194. Sien Tie S et al. *Mon. Not. R. Astron. Soc.* **515** 3656 (2022); arXiv:2201.10571
195. Mitchell R J et al. *Astrophys. J.* **200** L5 (1975)
196. Mitchell R J et al. *Mon. Not. R. Astron. Soc.* **175** 29P (1976)
197. Henriksen M J, Mushotzky R F *Space Sci. Rev.* **40** 681 (1985)
198. Henriksen M J, Mushotzky R F *Astrophys. J.* **302** 287 (1986)
199. Mushotzky R et al. *Astrophys. J.* **466** 686 (1996)
200. Renzini A, in *Clusters of Galaxies: Probes of Cosmological Structure and Galaxy Evolution, from the Carnegie Observatories Centennial Symp.* (Carnegie Observatories Astrophysics Ser., Vol. 260, Eds J S Mulchaey, A Dressler, A Oemler) (Cambridge: Cambridge University Press, 2004) p. 260; astro-ph/0307146
201. Mernier F et al. *Space Sci. Rev.* **214** 129 (2018)
202. Gu L et al. *Space Sci. Rev.* **214** 108 (2018)
203. Mernier F, Biffi V, in *Handbook of X-ray and Gamma-ray Astrophysics* (Eds C Bambi, A Santangelo) (Singapore: Springer, 2022) p. 1, https://doi.org/10.1007/978-981-16-4544-0_123-1; arXiv:2202.07097
204. Werner N et al. *Space Sci. Rev.* **134** 337 (2008)
205. Ettori S et al. *Astron. Astrophys.* **578** A46 (2015)
206. Sarkar A et al. *Mon. Not. R. Astron. Soc.* **516** 3068 (2022)
207. Péroux C, Howk J C *Annu. Rev. Astron. Astrophys.* **58** 363 (2020)
208. Peeples M S et al. *Astrophys. J.* **786** 54 (2014)
209. Tinsley B M *Fund. Cosmic Phys.* **5** 287 (1980)
210. Pettini M, in *Chemical Evolution from Zero to High Redshift* Vol. 233 (Eds J R Walsh, M R Rosa) (Berlin: Springer-Verlag, 1999); astro-ph/9902173
211. Cen R, Ostriker J P *Astrophys. J.* **514** 1 (1999)
212. Cen R, Ostriker J P *Astrophys. J.* **650** 560 (2006)
213. Ferrara A, Scannapieco E, Bergeron J *Astrophys. J.* **634** L37 (2005)
214. Bouché N et al. *Mon. Not. R. Astron. Soc.* **378** 525 (2007)
215. Sommer-Larsen J, Fynbo J P U *Mon. Not. R. Astron. Soc.* **385** 3 (2008)
216. Yates R M, Péroux C, Nelson D *Mon. Not. R. Astron. Soc.* **508** 3535 (2021)
217. Nicastro F et al. *Nature* **558** 406 (2018)
218. Schaye J et al. *Mon. Not. R. Astron. Soc.* **402** 1536 (2010)
219. Veilleux S, Cecil G, Bland-Hawthorn J *Annu. Rev. Astron. Astrophys.* **43** 769 (2005)
220. Bouché N et al. *Mon. Not. R. Astron. Soc.* **426** 801 (2012)
221. Bolatto A D et al. *Nature* **499** 450 (2013)
222. Rupke D S N, Veilleux S *Astrophys. J.* **768** 75 (2013)

223. Kompaneets A S *Sov. Phys. Dokl.* **5** 46 (1960); *Dokl. Akad. Nauk SSSR* **130** 1001 (1960)
224. Mac Low M M, McCray R, Norman M L *Astrophys. J.* **337** 141 (1989)
225. Igumenshchev I V, Shustov B M, Tutukov A V *Astron. Astrophys.* **234** 396 (1990)
226. Sarkar K C, Nath B B, Sharma P, Shchekinov Yu *Mon. Not. R. Astron. Soc.* **448** 328 (2015)
227. Babul A, Rees M J *Mon. Not. R. Astron. Soc.* **255** 346 (1992)
228. Ciardi B, Ferrara A *Astrophys. J.* **483** L5 (1997)
229. Murakami I, Babul A *Mon. Not. R. Astron. Soc.* **309** 161 (1999)
230. Mac Low M M, Ferrara A *Astrophys. J.* **513** 142 (1999)
231. D'Ercole A, Brighenti F *Mon. Not. R. Astron. Soc.* **309** 941 (1999)
232. Sharma M, Nath B B, Chattopadhyay I, Shchekinov Yu *Mon. Not. R. Astron. Soc.* **441** 431 (2014)
233. Sadoun R et al. *Astrophys. J.* **829** 71 (2016)
234. Fragile P C, Murray S D, Lin D N C *Astrophys. J.* **617** 1077 (2004)
235. Nath B B, Shchekinov Yu *Astrophys. J. Lett.* **777** L12 (2013)
236. Roy A, Nath B B, Sharma P, Shchekinov Yu *Mon. Not. R. Astron. Soc.* **434** 3572 (2013)
237. Kovalenko I G, Shchekinov Yu A *Astrophysics* **23** 578 (1985); *Astrofizika* **23** 363 (1985)
238. Strickland D K, Heckman T M *Astrophys. J.* **697** 2030 (2009)
239. von Glasow W et al. *Mon. Not. R. Astron. Soc.* **434** 1151 (2013)
240. Sharma P, Roy A, Nath B B, Shchekinov Yu *Mon. Not. R. Astron. Soc.* **443** 3463 (2014)
241. El-Badry K et al. *Mon. Not. R. Astron. Soc.* **490** 1961 (2019)
242. Shchekinov Yu A *Astron. Astrophys.* **314** 927 (1996)
243. Heiles C *Astrophys. J. Suppl.* **55** 585 (1984)
244. Heiles C *Astrophys. J.* **354** 483 (1990)
245. Koo B C, Heiles C, Reach W T *Astrophys. J.* **390** 108 (1992)
246. Melioli C et al. *Mon. Not. R. Astron. Soc.* **388** 573 (2008)
247. Melioli C et al. *Mon. Not. R. Astron. Soc.* **399** 1089 (2009)
248. Melioli C, de Gouveia Dal Pino E M, Geraissate F G *Mon. Not. R. Astron. Soc.* **430** 3235 (2013)
249. Melioli C, Brighenti F, D'Ercole A *Mon. Not. R. Astron. Soc.* **446** 299 (2015)
250. Vasiliev E O, Drozdov S A, Shchekinov Yu A *Open Astron.* **31** 99 (2022)
251. Leroy A K et al. *Astrophys. J.* **814** 83 (2015)
252. Veilleux S et al. *Astron. Astrophys. Rev.* **28** 2 (2020)
253. Bordoloi R et al. *Astrophys. J.* **796** 136 (2014)
254. Zhu G, Ménard B *Astrophys. J.* **770** 130 (2013)
255. Richter P et al. *Astron. Astrophys.* **590** A68 (2016)
256. Méndez-Hernández H et al. *Astron. Astrophys.* **666** A56 (2022); arXiv:2206.08923
257. Werk J K et al. *Astrophys. J.* **792** 8 (2014)
258. Zheng Y et al. *Astrophys. J.* **807** 103 (2015)
259. D'Odorico V et al. *Mon. Not. R. Astron. Soc.* **463** 2690 (2016)
260. Acharya A, Khaire V *Mon. Not. R. Astron. Soc.* **509** 5559 (2022)
261. Voit G M et al. *Nature* **519** 203 (2015)
262. Tumlinson J, Peeples M S, Werk J K *Annu. Rev. Astron. Astrophys.* **55** 389 (2017)
263. Donahue M, Voit G M *Phys. Rep.* **973** 1 (2022)
264. Barsella B et al. *Astron. Astrophys.* **209** 349 (1989)
265. Ferrara A et al. *Astrophys. J.* **381** 137 (1991)
266. Shustov B M, Vibe D Z *Astron. Rep.* **39** 578 (1995); *Astron. Zh.* **72** 650 (1995)
267. Bianchi S, Ferrara A *Mon. Not. R. Astron. Soc.* **358** 379 (2005)
268. Sharma M, Nath B B, Shchekinov Yu *Astrophys. J. Lett.* **736** L27 (2011)
269. Sivkova E E, Wiebe D S, Shustov B M *Astron. Rep.* **65** 370 (2021); *Astron. Zh.* **98** 363 (2021)
270. Sharma M, Nath B B *Astrophys. J.* **750** 55 (2012)
271. Hopkins P F, Quataert E, Murray N *Mon. Not. R. Astron. Soc.* **421** 3522 (2012)
272. Beck R *Space Sci. Rev.* **166** 215 (2012)
273. Ibáñez-Mejía J C et al. *Mon. Not. R. Astron. Soc.* **485** 1220 (2019)
274. Stein Y et al. *Astron. Astrophys.* **623** A33 (2019)
275. Mora-Partiarroyo S C et al. *Astron. Astrophys.* **632** A11 (2019)
276. Krause M et al. *Astron. Astrophys.* **639** A112 (2020)
277. Sokoloff D, Shukurov A *Nature* **347** 51 (1990)
278. Henriksen R N, Woodfinden A, Irwin J A *Mon. Not. R. Astron. Soc.* **476** 635 (2018)
279. Parker E N *Space Sci. Rev.* **9** 651 (1969)
280. Steinacker A, Shchekinov Yu A *Mon. Not. R. Astron. Soc.* **325** 208 (2001)
281. Heintz E, Bustard C, Zweibel E G *Astrophys. J.* **891** 157 (2020)
282. Hirashita H, Inoue A K *Mon. Not. R. Astron. Soc.* **487** 961 (2019)
283. Aoyama S et al. *Mon. Not. R. Astron. Soc.* **478** 4905 (2018)
284. Gnedin N Y, Ostriker J P *Astrophys. J.* **486** 581 (1997)
285. Gnedin N Y *Mon. Not. R. Astron. Soc.* **294** 407 (1998)
286. Bisnovatyi-Kogan G S, Silich S A *Rev. Mod. Phys.* **67** 661 (1995)
287. Suchkov A A et al. *Astrophys. J.* **430** 511 (1994)
288. Zu Y et al. *Mon. Not. R. Astron. Soc.* **412** 1059 (2011)
289. Oppenheimer B D, Davé R, Finlator K *Mon. Not. R. Astron. Soc.* **396** 729 (2009)
290. Vogelsberger M et al. *Mon. Not. R. Astron. Soc.* **444** 1518 (2014)
291. Pillepich A et al. *Mon. Not. R. Astron. Soc.* **473** 4077 (2018)
292. Pallottini A et al. *Mon. Not. R. Astron. Soc.* **513** 5621 (2022)
293. Kannan R et al. *Mon. Not. R. Astron. Soc.* **514** 3857 (2022)
294. Simcoe R A et al. *Astrophys. J.* **637** 648 (2006)
295. Tüllmann R et al. *Astron. Astrophys.* **457** 779 (2006)
296. Suchkov A A et al. *Astrophys. J.* **463** 528 (1996)
297. Mori M, Ferrara A, Madau P *Astrophys. J.* **571** 40 (2002)
298. Fujita A et al. *Astrophys. J.* **613** 159 (2004)
299. Marcolini A et al. *Mon. Not. R. Astron. Soc.* **371** 643 (2006)
300. Cooper J L et al. *Astrophys. J.* **674** 157 (2008)
301. Sarkar K C, Nath B B, Sharma P, Shchekinov Yu *Astrophys. J. Lett.* **818** L24 (2016)
302. Vasiliev E O, Nath B B, Shchekinov Yu *Mon. Not. R. Astron. Soc.* **446** 1703 (2015)
303. Vasiliev E O, Shchekinov Yu A, Nath B B *Mon. Not. R. Astron. Soc.* **468** 2757 (2017)
304. Kim C G, Ostriker E C *Astrophys. J.* **853** 173 (2018)
305. Klein R I, McKee C F, Colella P *Astrophys. J.* **420** 213 (1994)
306. Cooper J L et al. *Astrophys. J.* **703** 330 (2009)
307. Scannapieco E, Brüggen M *Astrophys. J.* **805** 158 (2015)
308. Schneider E E, Robertson B E *Astrophys. J.* **834** 144 (2017)
309. Zhang D et al. *Mon. Not. R. Astron. Soc.* **468** 4801 (2017)
310. Gronke M, Oh S P *Mon. Not. R. Astron. Soc.* **480** L111 (2018)
311. McCourt M et al. *Mon. Not. R. Astron. Soc.* **473** 5407 (2018)
312. Karitskaya E A et al., in *Why Galaxies Care about AGB Stars II: Shining Examples and Common Inhabitants. Proc. of a Conf., Vienna, Austria, 16–20 August 2010* (Astronomical Society of the Pacific Conf. Ser., Vol. 445, Eds F Kerschbaum, T Lebzelter, R F Wing) (San Francisco, CA: Astronomical Society of the Pacific, 2011) p. 335
313. Luck R E, Lambert D L *Astron J.* **142** 136 (2011)
314. Silva J V S et al. *Astrophys. J.* **901** 27 (2020)
315. De Cia A et al. *Nature* **597** 206 (2021)
316. Donnan C T, Tojeiro R, Kraljic K *Nat. Astron.* **6** 599 (2022)
317. Roy J R, Kunth D *Astron. Astrophys.* **294** 432 (1995)
318. Kraichnan R H *Phys. Fluids* **11** 945 (1968)
319. Kraichnan R H *J. Fluid Mech.* **64** 737 (1974)
320. Pan L, Scannapieco E *Astrophys. J.* **721** 1765 (2010)
321. Draine B T, Salpeter E E *Astrophys. J.* **231** 438 (1979)
322. Boselli A, Fossati M, Sun M *Astron. Astrophys. Rev.* **30** 3 (2022)
323. Shchekinov Yu A, Nath B B, Vasiliev E O *Universe* **8** 212 (2022)

324. Matvienko E E, Shchekinov Yu A *Astron. Astrophys. Trans.* **22** 317 (2003)
325. Evoli C, Ferrara A *Mon. Not. R. Astron. Soc.* **413** 2721 (2011)
326. Hasan F et al. *Astrophys. J.* **904** 44 (2020)
327. Campana S et al. *Astron. Astrophys.* **575** A43 (2015)
328. Bouché N, Lehnert M D, Péroux C *Mon. Not. R. Astron. Soc.* **364** 319 (2005)
329. Ferrara A, Pallottini A, Dayal P *Mon. Not. R. Astron. Soc.* **522** 3986 (2023); arXiv:2208.00720
330. Nath B B, Vasiliev E O, Drozdov S A, Shchekinov Yu A *Mon. Not. R. Astron. Soc.* **521** 662 (2023); arXiv:2211.12378
331. Shustov B et al. *Astrophys. Space Sci.* **363** 62 (2018)
332. Shustov B M *Astrophysics* **64** 405 (2021); *Astrofizika* **64** 455 (2021)
333. Boyarchuk A A et al. *Astron. Rep.* **60** 1 (2016); *Astron. Zh.* **93** 3 (2016)
334. Kardashev N S et al. *Phys. Usp.* **57** 1199 (2014); *Usp. Fiz. Nauk* **184** 1319 (2014)
335. Shchekinov Yu A et al. *Phys. Usp.* **60** 961 (2017); *Usp. Fiz. Nauk* **187** 1033 (2017)
336. Novikov I D et al. *Phys. Usp.* **64** 386 (2021); *Usp. Fiz. Nauk* **191** 404 (2021)
337. Vasiliev E O, Shchekinov Yu A, Nath B B *Astrophysics* **65** 324 (2022); *Astrofizika* **65** 333 (2022); arXiv:2003.14036
338. Larchenkova T I et al. *Astrophysics* **65** 161 (2022); *Astrofizika* **65** 179 (2022)
339. Gruppioni C et al. *Astron. Astrophys.* **643** A8 (2020)
340. Lupi A et al. *Mon. Not. R. Astron. Soc.* **496** 5160 (2020)
341. Pozzi F et al. *Astron. Astrophys.* **653** A84 (2021)